Neuron

Article

Encoding the glucose identity by discrete hypothalamic neurons via the gut-brain axis

Graphical abstract

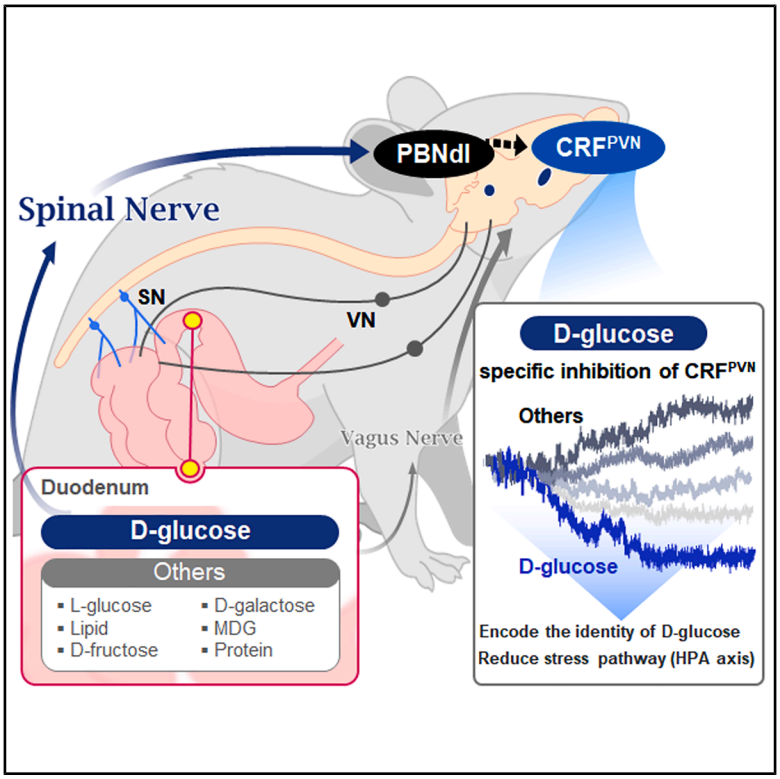

Highlights

- CRF^{PVN} neurons respond uniquely to intestinal D-glucose, distinct from other nutrients
- CRF^{PVN} neurons are essential for fasted mice to select D-glucose over other nutrients
- Fasting-activated PBNdl neurons are inhibited by D-glucose and excite CRF^{PVN} neurons
- D-glucose-evoked CRF^{PVN} response requires spinal nerves, not vagus nerves

Authors

Jineun Kim, Shinhye Kim, Wongyo Jung, ..., Young-Gyun Park, Gary J. Schwartz, Greg S.B. Suh

Correspondence

seongbaesuh@kaist.ac.kr

In brief

A specific neuronal population in the brain encoding D-glucose, the brain's main fuel, has been proposed but not yet identified. Kim et al. discovered a circuit involving CRF^{PVN} neurons, fasting-activated PBNdl neurons, and lumbar spinal neurons that together encode the identity of D-glucose, revealing a potential glucose-sensing neural pathway.

Kim et al., 2025, Neuron *113*, 2673–2691
August 20, 2025
https://doi.org/10.1016/j.neuron.2025.05.024

CellPress

Neuron

CellPress

Article

Encoding the glucose identity by discrete hypothalamic neurons via the gut-brain axis

Jineun Kim,[1,7,8] Shinhye Kim,[1,7] Wongyo Jung,[1,7,8] Yujin Kim,[1] Seongju Lee,[1] Sehun Kim,[2] Hae-Yong Park,[6] Dae Young Yoo,[5] In Koo Hwang,[5] Robert C. Froemke,[4] Seung-Hee Lee,[1,6] Young-Gyun Park,[2] Gary J. Schwartz,[3] and Greg S.B. Suh[1,9,*]

[1]Department of Biological Sciences, Korea Advanced Institute of Science and Technology, Daejeon 34141, Republic of Korea
[2]Department of Bio and Brain Engineering, Korea Advanced Institute of Science and Technology, Daejeon 34141, Republic of Korea
[3]Department of Medicine, Albert Einstein College of Medicine, 1300 Morris Park Avenue, Bronx, NY 10464, USA
[4]Department of Otolaryngology & Neuroscience Institute, New York University Grossman School of Medicine, 540 First Avenue, New York, NY 10016, USA
[5]Department of Anatomy and Cell Biology, College of Veterinary Medicine, Seoul National University, Seoul 08826, Republic of Korea
[6]Center for Synaptic Brain Dysfunctions, Institute for Basic Science, Daejeon 34141, Republic of Korea
[7]These authors contributed equally
[8]Present address: Department of Biology and Biological Engineering, California Institute of Technology, Pasadena, CA 91125, USA
[9]Lead contact
*Correspondence: seongbaesuh@kaist.ac.kr
https://doi.org/10.1016/j.neuron.2025.05.024

SUMMARY

Animals need daily intakes of three macronutrients: sugar, protein, and fat. Under fasted conditions, however, animals prioritize sugar as a primary source of energy. They must detect ingested sugar—specifically D-glucose—and quickly report its presence to the brain. Hypothalamic neurons that can respond to the caloric content in the gut regardless of the identity of macronutrient have been identified, but until now, the existence of neurons that can encode the specific macronutrients remained unknown. We found that a subset of corticotropin-releasing factor (CRF)-expressing neurons in the hypothalamic paraventricular nucleus (CRF^{PVN}) respond specifically to D-glucose in the gut, separately from other macronutrients or sugars. CRF^{PVN} neuronal activity is essential for fasted mice to develop a preference for D-glucose. These responses of CRF^{PVN} neurons to intestinal D-glucose require a specific spinal gut-brain pathway including the dorsal lateral parabrachial nuclei. These findings reveal the neural circuit that encodes the identity of D-glucose.

INTRODUCTION

Food-deprived animals across species need to be able to detect and consume foods rich in sugar calories to meet their energy needs. Among dietary sugars, glucose serves as the primary fuel source for organisms with brain cells that depend on it for energy.[1] The brain accounts for approximately 2% of body weight in humans, but it consumes roughly 20% of glucose-derived energy in the body.[2] Severe reductions in the brain glucose concentration can lead to serious health issues, including impairment of cognitive and reflex function, autonomic failure, and permanent brain damage.[1,3] To maintain a normal range of glucose concentration, particularly during a period of starvation, animals would monitor the glucose levels in their gastrointestinal tract[4] and distinguish it from other macronutrients such as lipids, proteins, or other carbohydrates that do not contain the glucose moiety.

Indeed, the information about nutrient contents in the gut is rapidly transmitted to the brain regions, one of which is the agouti-related peptide (AgRP)/neuropeptide Y (NPY) neuronal population in the arcuate nucleus of hypothalamus.[5–7] Hunger-responsive AgRP/NPY neurons are inhibited by the signals representing various types of nutrients—carbohydrates, proteins, and lipids—in the gut, possibly generalizing the total caloric content to the sensation of hunger in the arcuate nucleus. Notably, AgRP/NPY neuronal inhibition is proportional to the number of calories infused directly to the gut and is independent of the macronutrient identity.[5,6,8]

Natural sources of sugar reward the animal by providing a sweet taste and adequate caloric content, which are detected through taste-dependent and taste-independent modalities, respectively.[9–11] A series of seminal works suggests that a gastrointestinal system exists specifically for detecting the nutritional content of sugar and eliciting behaviors directed toward obtaining it.[12,13] The infusion of nutritive sugars directly into the stomach along with a neutral flavor induces a preference for that flavor without activating any orosensory cells.[14] Consistent with this, taste-blind trpm5(−/−) mice were able to respond to the nutritional value of sugar.[11] Recently, separate pathways in the dopaminergic reward system that encode nutritive sugar

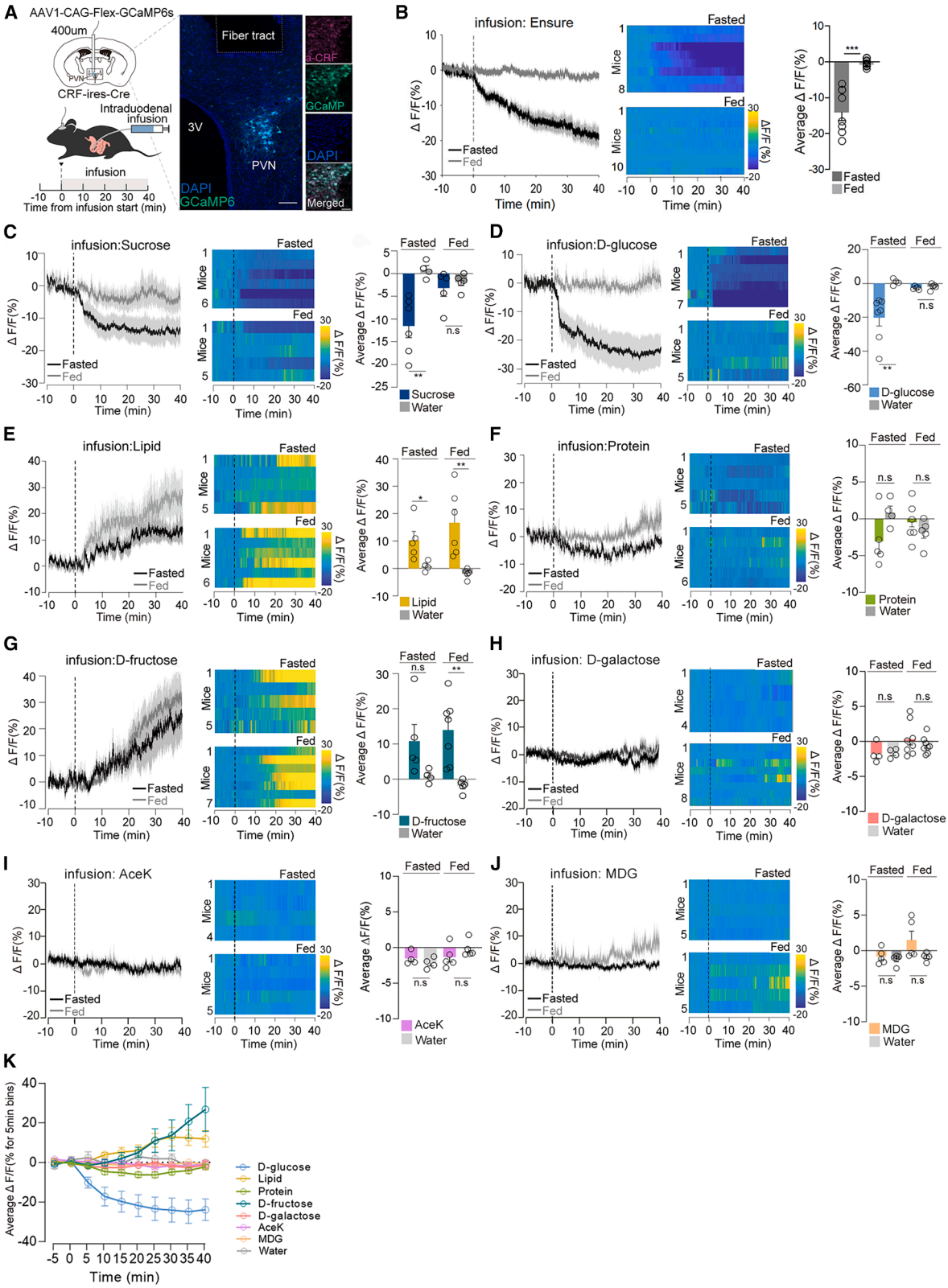

(legend on next page)

versus nonnutritive sweetener have been elucidated.[15] It is not clear, however, whether a neural encoding system that can distinguish D-glucose from qualitatively different macronutrients or other sugars exists.

Insight into this came from a Drosophila study. Taste-blind fruit flies, like taste-blind mice, can readily distinguish nutritive D-glucose from nonnutritive L-glucose under fasted conditions.[16–18] An unbiased GAL4 screen for cells required for responsiveness to D-glucose over L-glucose identified a population of six cells in the pars intercerebralis of the brain expressing the diuretic hormone 44 peptide (DH44). These DH44 neurons play a pivotal role in allowing animals to distinguish between nutritive and nonnutritive sugars and promoting sugar consumption during starvation.[18,19] Notably, the activity of DH44 neurons is robustly stimulated by D-glucose, but not by L-glucose, different macronutrients, or other nutritive sugars, underlining the specificity of D-glucose. In the light of the homology between DH44 in Drosophila and corticotropin-releasing factor (CRF) in mammals,[20] we hypothesized that CRF neurons in the paraventricular nucleus (PVN) of the hypothalamus are important for mediating the detection and consumption of D-glucose in mice under fasted conditions.

CRF neurons in the PVN (CRF^{PVN}) of the hypothalamus stimulate the hypothalamic-pituitary-adrenal (HPA) axis to produce glucocorticoids in response to physical or psychological stress.[21] These glucocorticoids help maintain glucose homeostasis by directing counterregulatory responses (CRRs) during prolonged starvation.[22] Beyond the HPA axis, CRF^{PVN} neurons mediate diverse functions, influencing acute stress behaviors,[23] responses to aversive and rewarding sensory stimuli,[24] stress control and defensive behavior regulation,[25] and social behaviors via the gut microbiome.[26] To support these functions, CRF^{PVN} neurons receive abundant inputs from various parts of the brain.[27,28]

In this work, we found that a subset of CRF^{PVN} neurons uniquely and acutely respond to intestinal D-glucose, promoting the consumption of D-glucose. Perturbing CRF^{PVN} neuronal activity impaired the preference for D-glucose-containing sugars in fasted mice. Using fiber photometry and gradient refractive index (GRIN)-lens-guided single-cell imaging, we observed that D-glucose-containing sugars infused into the proximal intestine rapidly inhibited CRF^{PVN} neurons, distinguishing their response from nonnutritive sugars, lipids, proteins, or sugars lacking the D-glucose moiety. We delineated the peripheral neural pathways that convey gut nutrient signals to CRF^{PVN} neurons and found that a subpopulation of the dorsal lateral parabrachial nuclei (PBNdl) form monosynaptic connections to CRF^{PVN} neurons and spinal nerves. This neural circuit is required for CRF^{PVN} neurons to respond to D-glucose in the gut. Together, we propose that intestinal D-glucose is recognized by a subset of the brain CRF^{PVN} neurons that are recruited to encode this brain fuel during fasting, which may help temper the hypoglycemia-induced activation of the HPA axis.

RESULTS

D-glucose infused into the gut rapidly inhibits CRF^{PVN} neuronal activity

We first tested the possibility that the intake of nutritive sugar modulates the activity of CRF^{PVN} neurons. We previously reported that the orosensory detection of food initially suppressed CRF^{PVN} neuronal activity, which remained to be inhibited after food was consumed.[24] This observation led us to hypothesize that a signal representing the presence of nutrients in the gastrointestinal tract directs the significant inhibition of CRF^{PVN} neuronal activity independently of the actions driven by the orosensory modality. To this end, we applied an approach to deliver nutrients directly into the upper intestine, duodenum, where nutrients begin to be absorbed, through an implanted catheter at an infusion rate of 15 μL/min[29–31] over 40 min (for a total infusion of 600 μL) while simultaneously recording GCaMP6s fluorescence signals from CRF^{PVN} neurons via *in vivo* fiber photometry in freely moving mice (Figure 1A). We observed that the intraduodenal (ID) infusion of a nutritionally complete liquid diet (Ensure, 1.2 kcal/mL) at the rate of 15 μL/min resulted in robust and sustained inhibition of CRF^{PVN} neuronal activity. This response was more substantial in fasted mice than in fed mice (Figure 1B). These results demonstrate that nutrients infused directly into the intestine without orosensory stimulation have a potent effect on the activity of CRF^{PVN} neurons in the brain.

To identify specific macronutrients responsible for the strong inhibitory effect on CRF^{PVN} neurons, we infused isovolumetric amounts of water, sucralose, and isocaloric nutritive sugars as well as lipids and protein into the duodenum. Neither water nor nonnutritive sucralose, which may not be absorbed in circulation,[32] altered CRF^{PVN} neuronal activity in fed or fasted mice (Figures S1A and S1B), but the nutritive sugar (30% of sucrose) significantly inhibited CRF^{PVN} neuronal activity, particularly under fasted conditions (Figure 1C). Consistent with this, CRF^{PVN} neuronal activity was strongly suppressed following the ID infusion of isocaloric nutritive 30% D-glucose under fasted conditions (Figures 1D, 1K, and S1C–S1E). This effect became

Figure 1. Distinct CRF^{PVN} neuronal response to D-glucose-containing sugars

(A) Schematic of fiber photometry setup: optic fiber and AAV-GCaMP6s injection in the PVN of *Crf-IRES-Cre* mice (left upper). *In vivo* recording during intraduodenal (ID) infusion (15 μL/min for 40 min). Right: GCaMP6s expression and fiber tract (scale bar, 100 μm); co-localization of GCaMP6s (green) and CRF (red) (90.3% for cells with CRF+GCaMP6+/GCaMP6+, $N = 2$ mice).

(B–J) Peri-stimulus time histograms (PSTH) plots (left), heatmaps (middle), and quantifications (right) of ΔF/F(%) of GCaMP6s signals in CRF^{PVN} neurons ($CRF^{PVN:GCaMP6}$ signals) aligned to the onset of ID infusion of Ensure (B), sucrose (C), D-glucose (D), lipid (E), protein (F), D-fructose (G), or D-galactose (H) with the same 1.2 kcal/mL calories, equal to 30% D-glucose (B–H), 30 mM AceK (I), or 30% MDG (J), nonnutritive sweeteners (I and J). Dashed lines indicate infusion onset. Bold lines and shaded areas denote the mean and SEM, respectively. Light circles: individual mice. $\Delta F/F(\%) = (F_{during\ infusion} - F_{baseline})/(F_{baseline}) \times 100$.

(K) Summary of time-binned average ΔF/F(%) of $CRF^{PVN:GCaMP6}$ signals during 5-min intervals throughout ID infusion.

Two-way ANOVA with Holm-Sidak multiple comparison in this and subsequent figures unless indicated otherwise: $^{*}p < 0.05$, $^{**}p < 0.01$, and $^{***}p < 0.001$. n.s., non-significant. See statistical details in Table S1. Mean ± SEM.

See also Figure S1.

statistically significant only after approximately 20 mg of D-glucose in a solution had been infused (mean latency to inhibition period: 4.3 ± 0.5 min following the infusion of 30% D-glucose at a rate of 15 μL/min; total intake: 19.35 mg; Figure S1E, inset). By contrast, the ID infusion of 30% nonnutritive L-glucose had the opposite effect on the activity of CRF^{PVN} neurons, increasing the GCaMP signal in CRF^{PVN} neurons substantially in both fasted and fed mice (Figures S1F–S1H).

To determine whether the D-glucose-induced inhibition of CRF^{PVN} neuronal activity reflects the number of infused calories, regardless of the type or quality of macronutrients, we infused a solution of 13.3% intralipids or a solution of 30% protein (each of which was isocaloric to the previously infused 30% D-glucose) into the duodenum of each mouse while recording the activity of CRF^{PVN} neurons. None of these infusions caused a reduction in the activity of CRF^{PVN} neurons. Instead, the infused lipids stimulated the activity of CRF^{PVN} neurons acutely and substantially in both fasted and fed states (Figures 1E and 1K), but the isocaloric protein solution (a complex mixture) did not have a significant effect on CRF^{PVN} neuronal activity (Figures 1F and 1K). Because the CRF^{PVN} neuronal response to D-glucose and sucrose was distinct from their response to other macronutrients, we investigated the possibility that an ID infusion of the other monosaccharide component of sucrose, D-fructose, would have a similar response. Infused isocaloric 30% D-fructose did not reduce the activity of CRF^{PVN} neurons in either fed or fasted mice but unexpectedly triggered a robust increase in CRF^{PVN} neuronal activity (Figure 1G), similar to that seen with nonnutritive L-glucose (Figures S1F–S1H). The ID infusion of 30% D-galactose neither reduced nor stimulated the activity of CRF^{PVN} neurons in fed or fasted mice (Figure 1H). Similarly, other nonnutritive sweeteners such as 30 mM acesulfame potassium (AceK),[33] 30% α-methyl-D-glucopyranoside (MDG),[8] and 500 mM D-Mannitol[33] did not inhibit or activate CRF^{PVN} neurons in fed or fasted mice (Figures 1I–1K and S1R–S1T). These sweeteners, however, may not be absorbed into circulation efficiently and therefore did not result in a change in the activity of CRF^{PVN} neurons.

The magnitude and persistence of CRF^{PVN} GCaMP signals were less pronounced in lower concentrations of all infusates (Figures S1C–S1E and S1I–S1T); however, the inhibition of CRF^{PVN} neuronal activity, specifically by duodenal D-glucose, was unambiguously observed even at lower concentrations (Figure S1U). These results support the hypothesis that CRF^{PVN} neurons can distinguish intestinal D-glucose or D-glucose-containing sugars, which are used as fuel by the brain cells, from other macronutrients including lipids, proteins, and sugars that do not contain the D-glucose moiety.

The observation that CRF^{PVN} neurons respond rapidly and uniquely to duodenal D-glucose under fasted conditions led us to investigate how nutrient information in the gut is transmitted to CRF^{PVN} neurons in the brain. To determine whether the inhibitory effect of infused D-glucose on CRF^{PVN} neurons takes place at the pre-absorptive site of the intestinal lumen or after it has been absorbed through the intestinal walls (i.e., across the epithelial enterocytes), we co-infused D-glucose with one of two D-glucose transporter blockers—phlorizin for sodium-glucose co-transporter (SGLT1/2) or phloretin for glucose transporter 2 (GLUT2)—or a mixture of these two blockers.[34] These treatments completely attenuated the glucose-evoked inhibition of CRF^{PVN} neuronal activity (Figures 2A–2G), suggesting that the ability of duodenal D-glucose to inhibit CRF^{PVN} neuronal activity depends on the post-absorptive signaling of D-glucose. These findings are consistent with previous studies indicating that D-glucose is transported from the lumen of the intestine to circulation by SGLT1 and GLUT2.[35,36] This transport mechanism is distinct from those for D-fructose and lipid and may be linked to the opposing responses generated by CRF^{PVN} neurons (see Figures 1D, 1E, and 1G).

Nutrients in the intestinal lumen are known to induce the release of several satiety hormones or the activation of extrinsic afferent nerves.[37,38] Therefore, we decided to explore the possible effects of humoral signals on CRF^{PVN} neurons. The activity of CRF^{PVN} neurons was indeed augmented following an intraperitoneal (i.p.) injection of the orexigenic hunger hormone ghrelin into mice that had been fed *ad libitum* but suppressed after a subsequent ID infusion of D-glucose (Figure 2H). This is consistent with the inhibitory effect of ID-infused D-glucose on CRF^{PVN} neuronal activity under fasted conditions (Figures 2H–2J; see Figure 1D). However, CRF^{PVN} neuronal activity was not modulated by i.p. injections of anorexigenic gastrointestinal hormones, including cholecystokinin (CCK), peptide YY (PYY), amylin, or a glucagon-like peptide-1 (GLP1) agonist, liraglutide, in fasted mice (Figures 2K–2S). These results suggest that changes in the levels of the gastrointestinal satiety peptides may not directly influence the activity of CRF^{PVN} neurons. This provides additional support that CRF^{PVN} neuronal activity is not affected by the humoral satiety signals but, rather, incorporates a specific mechanism that allows CRF^{PVN} neurons to rapidly distinguish ingested D-glucose from other nutrients in the gut.

Operant self-infusion of duodenal D-glucose is blunted by the acute stimulation of CRF^{PVN} neuronal activity

Having demonstrated that duodenal D-glucose suppressed CRF^{PVN} neuronal activity without orosensory stimulation, we sought to determine whether CRF^{PVN} neuronal activity is operationally important for mediating the moment-to-moment intake of D-glucose and provides positive reinforcement. In previous studies, it was reported that mice could learn to lick at a dry spout to obtain the ID infusions of D-glucose and other macronutrients.[14,39] We investigated the functional relevance of CRF^{PVN} neuronal activity during the operant dry-licking assay for the ID infusion of nutritive D-glucose versus nonnutritive L-glucose or isocaloric lipids. To this end, food-restricted mice were trained to lick a spout baited with a small piece of food for 3 days. Whenever the mice licked the baited spout, an ID infusion of Ensure (0.6 kcal/mL) was delivered over 3 s at a rate of 5 μL of infusion per lick (Figure 3A upper).

The trained, fasted mice were subjected to test sessions during which licking a dry spout triggered the ID infusion of D-glucose (1.2 kcal/mL), an iso-concentration of L-glucose, or isocaloric lipids (Figure 3A, lower). We next monitored the CRF^{PVN} neuronal response during the operant dry-licking assay using fiber photometry. Notably, GCaMP6s fluorescence signals from CRF^{PVN} neurons were rapidly suppressed from the onset of each licking bout that triggered the ID infusion of D-glucose

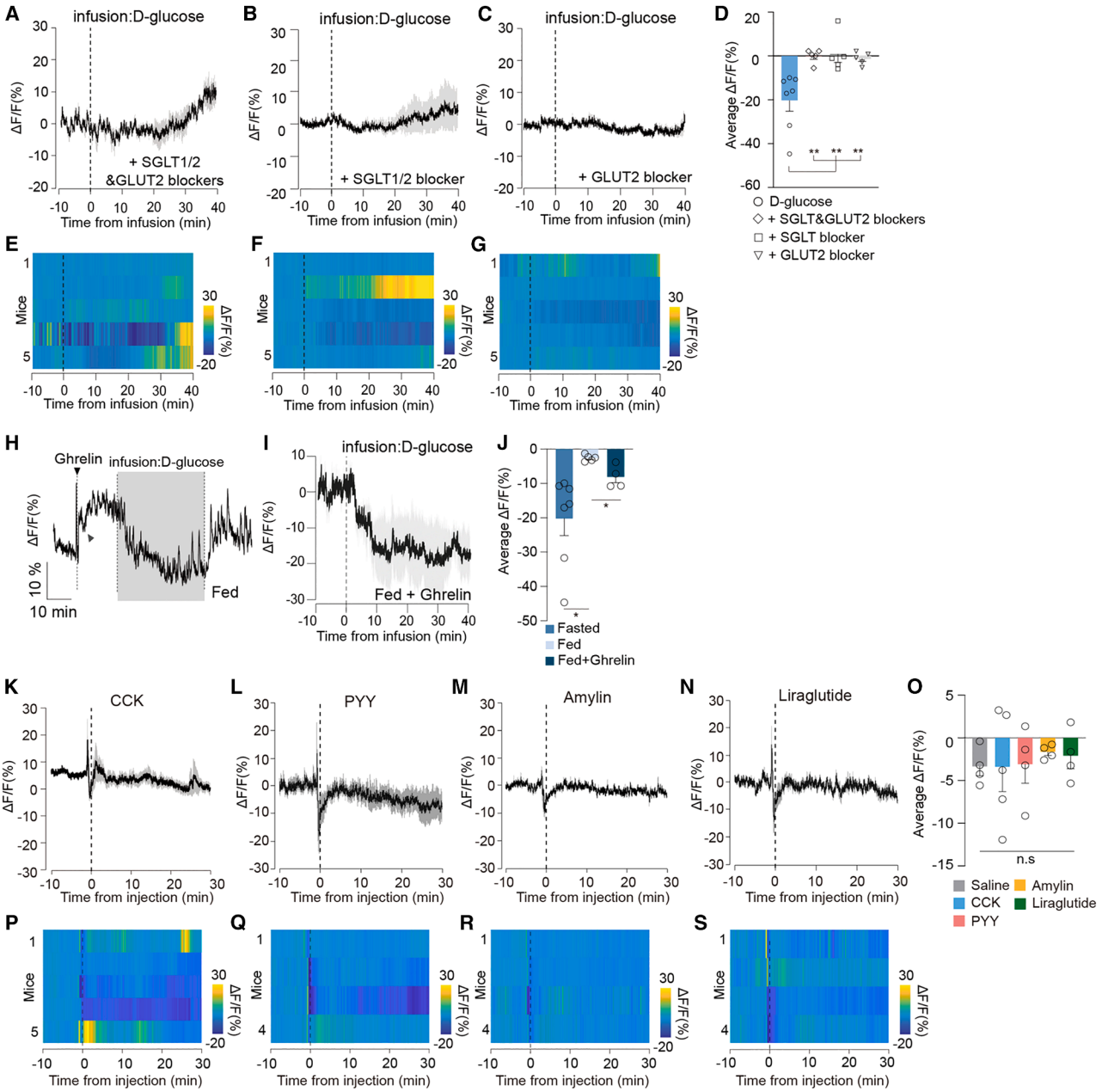

Figure 2. D-glucose-induced CRF^{PVN} neuronal inhibition depends on hunger state and glucose transporters, not satiety hormones

(A–G) PSTH plots (A–C), heatmaps (E–G), and quantifications (D) of ΔF/F(%) of *CRF$^{PVN:GCaMP6}$* signals aligned to the onset of co-infusion of 30% D-glucose with phloridzin (SGLT1 blocker) or/and phloretin (GLUT2 blocker) in 20-h fasted mice ($N = 5$).

(H–J) Representative trace showing *CRF$^{PVN:GCaMP6}$* activation by ghrelin (i.p.) in fed mice, followed by inhibition with D-glucose infusion (H). PSTH plots of ΔF/F (%) of *CRF$^{PVN:GCaMP6s}$* response to D-glucose post-ghrelin ($N = 4$ mice) (I). Group comparison: fasted, fed, and ghrelin-treated fed mice (J).

(K–S) PSTH plots (K–N), heatmaps (P–S), and quantifications (O) of ΔF/F(%) of *CRF$^{PVN:GCaMP6}$* signals aligned to the onset of i.p. injection of satiety hormones, CCK (K and P), PYY (L and Q), amylin (M and R), or liraglutide (N and S) in fasted mice.

*$p < 0.05$ and ** $p < 0.01$.

(Figures 3B upper, 3C, and 3F). By contrast, GCaMP6s signals from CRF^{PVN} neurons were rapidly stimulated at the onset of each licking bout for infused L-glucose or lipids (Figures 3B middle and lower and 3D–3F). These calcium imaging experiments using a dry-lick conditioned stimulus further support the distinct calcium dynamics of CRF^{PVN} neurons in response to different infused nutrients.

We further sought to determine whether the acute, transient suppression of CRF^{PVN} neuronal activity by infused D-glucose is required for the continuous engagement of appetitive

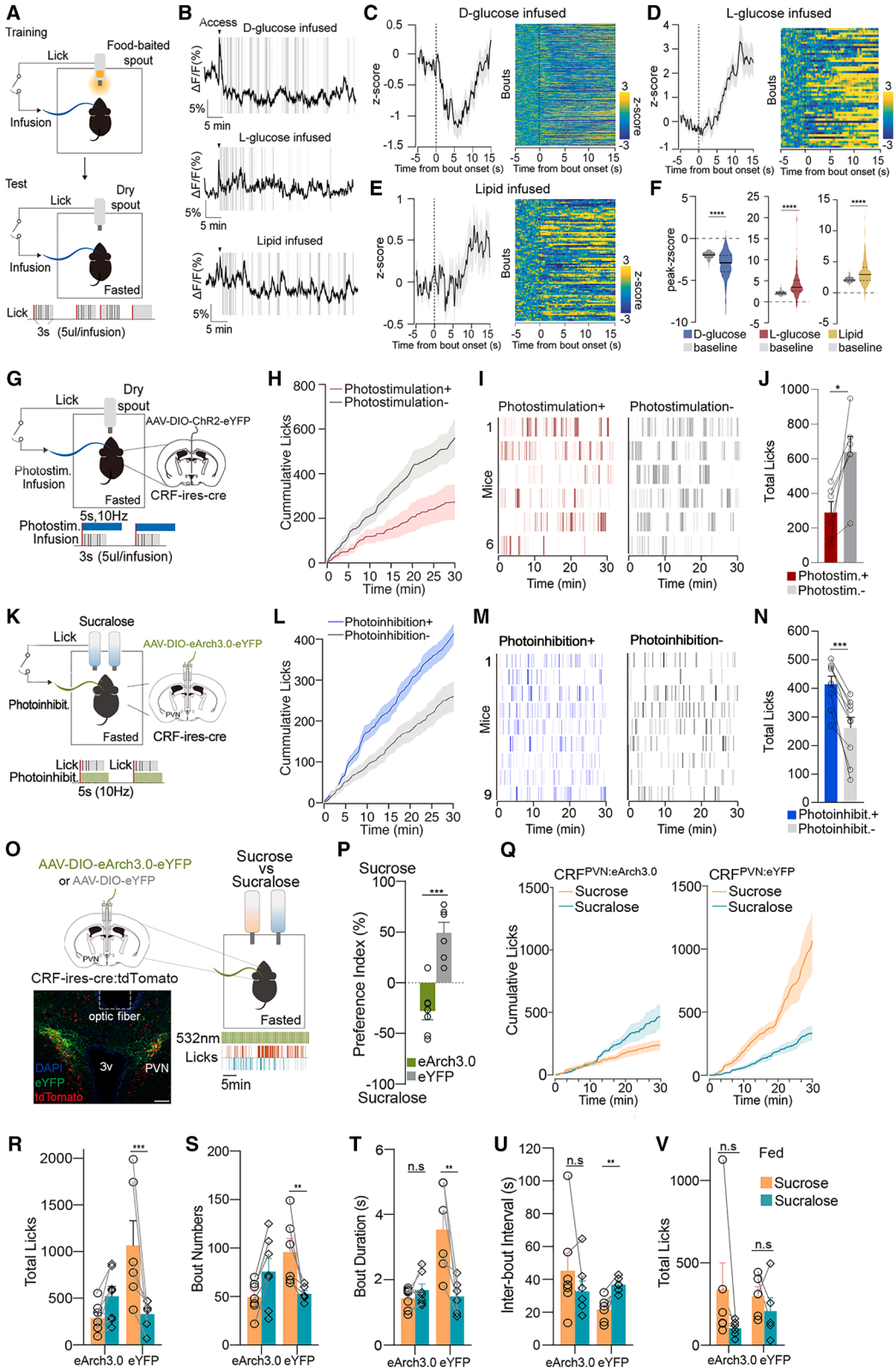

(legend on next page)

behavior: dry licking. To do so, we artificially stimulated CRF^{PVN} neuronal activity through optogenetic method when mice displayed dry licks; this also triggered the ID infusion of D-glucose (Figure 3G). The artificial stimulation of CRF^{PVN} neurons triggered by dry licking was followed by a significant attenuation of dry licking compared with the effect of a session without photostimulation, despite the simultaneous ID infusion of D-glucose (Figures 3H–3J). Consistent with this, artificial inhibition of CRF^{PVN} neurons at the onset of each licking bout rendered a preference for a sucralose-containing bottle paired with lick-triggered photoinhibition over another sucralose-containing bottle without photoinhibition (Figures 3K–3N). Thus, the operant conditioning paradigm supports the importance of D-glucose-evoked inhibition of CRF^{PVN} neuronal activity for the positive reinforcement of D-glucose intake during the fasted state.

CRF^{PVN} neuronal activity is required for fasting-induced behavioral responses to D-glucose

We next determined whether CRF^{PVN} neurons are important for responding to nutritive D-glucose without conditioning. To this end, we designed a two-choice assay in which naive mice (i.e., mice that had not been exposed to a plain sugar solution) were given a choice between a bottle (with spout) containing a 100-mM solution of nutritive sucrose and another bottle (with spout) containing a 0.5-mM solution of nonnutritive sucralose (the chosen concentrations rendered an equal preference in fed mice—data not shown) under fed or fasted conditions (Figure S2A). The concentration of sucrose was similar to the concentration found in the chow diet that the mice consumed daily.[40] The amount of each solution consumed was measured manually every 1 h during the dark cycle. *Ad libitum*-fed mice showed no preference for sucrose over sucralose during the first few hours but gradually started consuming more sucrose than sucralose within 4–6 h after the assay began (Figure S2B, gray line). During this period, no other food was provided. After 20 h of fasting, mice consumed significantly larger amounts of sucrose than sucralose within 1 h of feeding (Figure S2B, black line).

Having established a behavioral assay that can be used to measure the fasting-induced preference for nutritive sugar, we investigated the possibility that CRF^{PVN} neurons are required for mediating this preference under fasted conditions. We found that mice in which CRF^{PVN} neurons had been ablated using diphtheria toxin (*Crf-IRES-Cre*—crossed to inducible diphtheria toxin receptor, *iDTR* mice)[41] failed to select nutritive sugar over nonnutritive sweetener in the two-choice assay, while control mice (iDTR only) developed a preference for nutritive sugar (Figure S2C). We also found that chemogenetic silencing of CRF^{PVN} neuronal activity in fasted *Crf-IRES-Cre* mice that had received bilateral injections of adeno-associated virus (AAV)-double-floxed inverted open reading frame (DIO)-hM4Di-mCherry into the PVN ($CRF^{PVN:hM4Di\text{-}CNO}$ mice) abolished the preference and consumption of sucrose upon receiving an i.p. injection of clozapine-N-oxide (CNO) before the assay but had no effect on the consumption of sucralose (Figures S2D–S2F).

Because the fasting-induced preference for nutritive sugar became significant within 1 h, we employed a short-term, two-choice assay to determine whether optogenetic manipulations of CRF^{PVN} neurons can alter this preference. We injected AAV viruses bearing the Cre-inducible DIO-eArch3.0-eYFP to induce optogenetic inhibition of CRF^{PVN} neuronal activity (Figure 3O, left). Each injection was made bilaterally into the PVN of *Crf-IRES-Cre* mice bearing *Rosa-loxpSTOPloxp-tdTomato* (*Ai14*) mice. The feeding behaviors of these mice were evaluated using lickometers, which automatically count licking events on a millisecond scale (Figure 3O, right). Fasted, naive mice that

Figure 3. CRF^{PVN} neuronal activity is required for the positive reinforcement of D-glucose during operant self-infusion

(A) Schematic of the operant dry-spout lick-triggered ID infusion paradigm. After 3 days of training with Ensure, 16-h fasted mice licked a dry spout to trigger ID infusion of D-glucose, L-glucose, or lipid. The first lick in a bout (red lines) triggered a 5-μL infusion (gray box) for 3 s; licks during infusion (black lines) did not trigger additional delivery.

(B) Representative traces of $CRF^{PVN:GCaMP6}$ signals during operant dry-spout licking for D-glucose, L-glucose, and lipid. Shaded bars depict the licking event; arrowheads denote spout access onset.

(C–E) Population peri-event time histograms (PETH) plots and heatmaps of Z scored $CRF^{PVN:GCaMP6}$ signals aligned to bout onset with D-glucose (C), L-glucose (D), and lipid (E) infusion.

(F) Quantification of peak Z scores 15 s after D-glucose, L-glucose, and lipid infusion. Center lines, median; dashed lines, lower, and upper quartiles; **** $p < 0.001$, two-tailed paired t test.

(G) Schematic of lick-triggered ID infusion of D-glucose paired with optogenetic activation of CRF^{PVN} neurons (473 nm, 10 Hz, and 10 ms pulses for 5 s) initiated by the first lick (red lines) in a bout.

(H–J) Cumulative lick counts (H), raster plots of licking (I), and quantification of the total licks during 30 min of the operant dry licking (J) for D-glucose in fasted $CRF^{PVN:ChR2}$ mice. Student's paired t test, * $p < 0.05$.

(K) Schematic illustrating the two-choice assay where one of the two identical bottles containing sucralose is paired with optogenetic inhibition (532 nm, 10 Hz, and 10 ms pulses for 5 s) at first lick (red lines).

(L–N) Cumulative sucralose lick counts (L), raster plots of licking (M), and quantification of the total licks during 30 min of the two-choice test in fasted $CRF^{PVN:eArch3.0}$ mice. Student's paired t test, *** $p = 0.0002$.

(O) Schematic of AAV-mediated Cre-dependent eArch3.0 or enhanced yellow fluorescent protein (eYFP) expression and optic fiber implantation into the PVN (left). Representative eArch3.0-eYFP expression image (lower left; scale bar, 100 μm). Schematic of two-choice assay (100 mM sucrose versus 0.5 mM sucralose) and example licking raster plot under continuous photoinhibition (532 nm, green bar) (right).

(P) Sucrose preference index (%) during continuous photoinhibition in fasted $CRF^{PVN:eArch3.0}$ ($N = 6$) and eYFP ($N = 6$) mice.

(Q) Cumulative lick counts for sucrose and sucralose in fasted $CRF^{PVN:eArch3.0}$ and $CRF^{PVN:eYFP}$ mice during the two-choice assay.

(R–U) Additional lick metrics during the two-choice assay: total licks (R), bout numbers (S), bout duration (T), and inter-bout intervals (U).

(V) Total licks in fed $CRF^{PVN:eArch3.0}$ ($N = 6$) and $CRF^{PVN:eYFP}$ ($N = 5$) mice.

** $p < 0.01$ and *** $p < 0.001$ (R–U).

See also Figure S2.

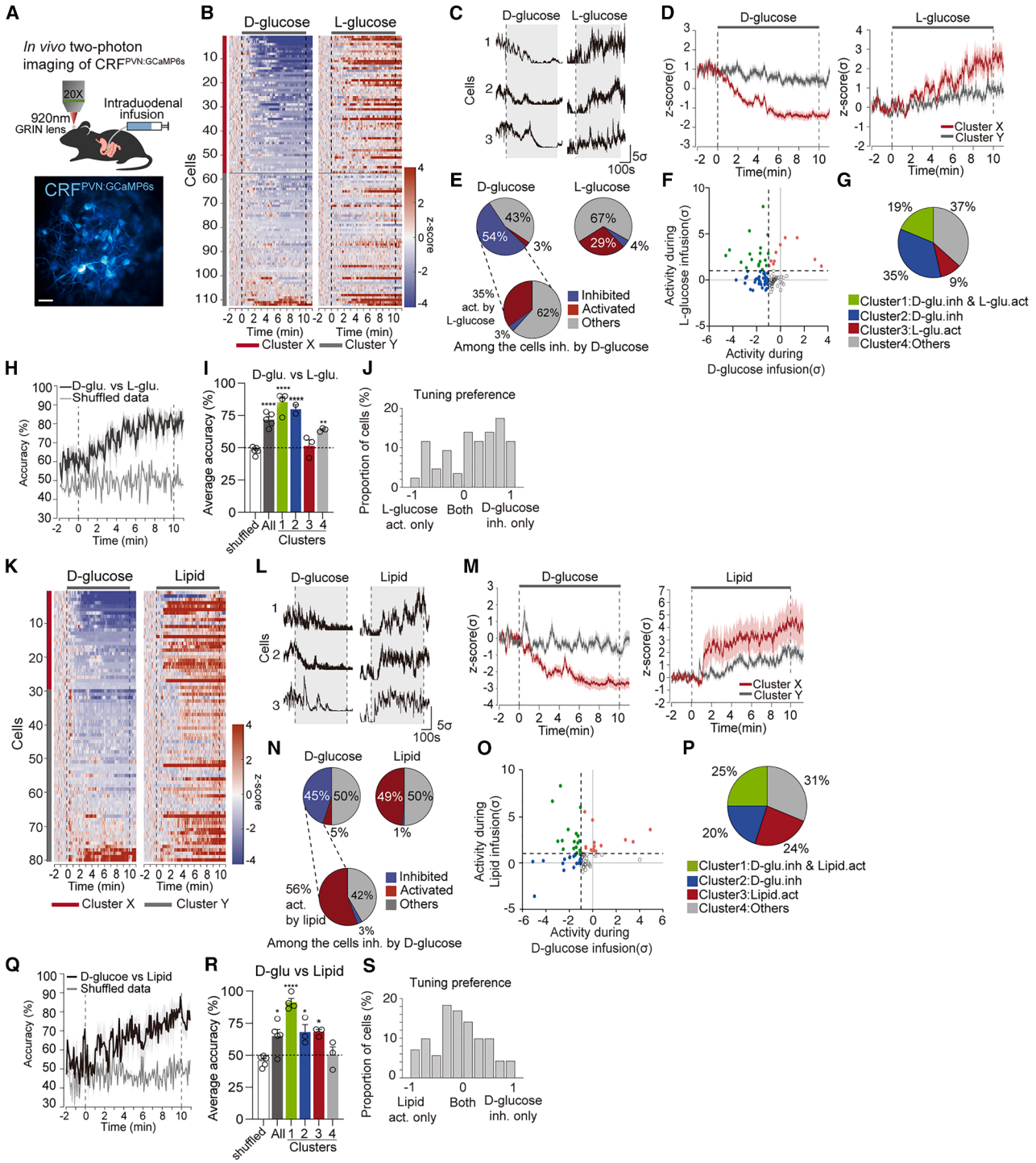

Figure 4. A subpopulation of CRF^{PVN} neurons responds to gut nutrients

(A) Schematic showing the setup for single-cell two-photon imaging of *CRF$^{PVN:GCaMP6}$* during ID infusions (10 min and 15 μL/min) in head-fixed mice (upper). Representative GRIN lens image of individual CRF^{PVN} neurons (lower). Scale bar, 50 μm.

(B and K) Heatmaps depicting *Z* scored *CRF$^{PVN:GCaMP6}$* activity from individual neurons of fasted mice during sequential ID infusions of 30% D-glucose and 30% L-glucose (B) or 30% D-glucose and isocaloric lipid (K) (D-glucose and L-glucose: $n = 112$ cells, 5 mice; D-glucose and lipid: $n = 80$ cells, 5 mice). Solid-colored lines indicate clusters identified by unsupervised k-means clustering; dashed lines indicate the onset and offset of ID infusion.

(C and L) Representative traces illustrating calcium dynamics of CRF^{PVN} neurons bidirectionally responding to D-glucose and L-glucose (C) or D-glucose and lipid (L). Gray shaded areas mark the 10-min infusion periods.

(legend continued on next page)

expressed the control AAV-DIO-eYFP in the PVN (*CRF*$^{PVN:eYFP}$ mice) rapidly developed a preference for sucrose over sucralose and started consuming more sucrose than sucralose within 10 min after the assay began, regardless of whether they had been stimulated (Figures 3P–3R). The number of licking bouts and the duration of each bout for sucrose increased significantly (Figures 3S and 3T), and the inter-bout interval decreased significantly (Figure 3U). This is consistent with the view that fasted mice prefer and consume more nutritive sugar. By contrast, fasted mice in which CRF^{PVN} neuronal activity was optogenetically silenced (*CRF*$^{PVN:eArch3.0}$ mice) during 30 min of the two-choice assay failed to select sucrose over sucralose and consumed less sucrose than sucralose (Figures 3P–3R). Consistent with this, the number of licking bouts, the duration of each bout, and the inter-bout interval for sucrose were not significantly different from those for sucralose (Figures 3S–3U).

Notably, we found that optogenetic inhibition of CRF^{PVN} neurons did not influence the total sucrose intake in fed mice (Figure 3V), suggesting that these neurons likely play an important role in sucrose consumption only under fasted conditions. Moreover, the inhibition of CRF^{PVN} neuronal activity significantly reduced the intake of sucrose in fasted mice (Figure 3R) but did not affect the intake of chow food, which contains other macronutrients in addition to sugars (Figure S2G). This observation is consistent with a previous report indicating that the activity of CRF^{PVN} neurons does not regulate acute food intake or body weight in general.[42,43] These lines of evidence support the hypothesis that CRF^{PVN} neuronal activity is important for the selection and consumption of sugar, but not necessarily other macronutrients, only during periods of food deprivation.

We next sought to determine whether the impairment in fasting-induced sugar preference caused by silencing of CRF^{PVN} neurons was caused by a defect in the secretion of CRF peptides, which is known to stimulate the HPA axis.[44,45] To do so, we conditionally knocked out *Crf* gene by injecting the AAV1-Cre-GFP virus bilaterally into the PVN of *Crf*$^{lox/lox}$ (*PVN*$^{Crf\text{-}KO}$ mice) or *Crf*$^{lox/+}$ control mice (Figure S2H).[46] Successful deletion of *Crf* was validated by the loss of anti-CRF immunoreactivity in the PVN of *PVN*$^{Crf\text{-}KO}$ mice, as was observed in the PVN of *Crf*$^{lox/+}$ control mice (Figure S2H, middle, and right). Unlike the defect observed in mice in which CRF^{PVN} neuronal activity had been manipulated, the fasting-induced preference for nutritive sugar was not impaired in *PVN*$^{Crf\text{-}KO}$ mice (Figures S2I and S2K). Consistent with this finding, a bilateral adrenalectomy performed to halt the release of corticosteroid hormone (CORT—a key conveyor of the HPA axis)[47] did not impair the preference for nutritive sugar under fasted conditions (Figures S2J and S2K). These results indicate that the activity of CRF^{PVN} neurons, but not necessarily CRF peptide or HPA axis per se, is important for mediating the fasting-induced preference and consumption of sugar.

A subset of CRF^{PVN} neurons respond to intestinal nutrients

Since CRF^{PVN} neuronal activity at a population level, recorded via fiber photometry, was inhibited by D-glucose and D-glucose-containing sugars but stimulated by lipids, L-glucose, and D-fructose, we asked whether specific CRF^{PVN} subpopulations selectively respond to nutrients. Using single-cell calcium imaging with two-photon microscopy through GRIN lens implanted above the PVN in awake, head-fixed mice with ID catheters, we monitored GCaMP6s signals from individual CRF^{PVN} neurons during nutrient infusion (Figure 4A). Fasted mice (18 h) received ID infusions of iso-concentration L-glucose, isocaloric D-glucose, lipids, protein, or D-fructose (1.2 kcal/mL) in randomized order. To track the same field of view and co-register cells across different imaging sessions, we compared calcium dynamics of CRF^{PVN} neurons imaged on the same day or within an interval of a few days and allowed an interval of at least 20 min to prevent carryover effects (see STAR Methods).

We found that the majority of imaged CRF^{PVN} neurons in fasted mice were inhibited by infused D-glucose (Figures 4B, 4C, and 4E-left; inhibited: 54%, activated: 3%, others: 43%; $n = 112$ cells), but activated by L-glucose (Figures 4B, 4C, and 4E-right; activated: 29%, inhibited: 4%, others: 67%; $n = 112$ cells). Some classified as "others" showed minor responses (Figures 4E–4G). Notably, approximately 35% of the D-glucose-inhibited CRF^{PVN} neurons were activated by L-glucose. K-means clustering confirmed a subpopulation inhibited by D-glucose but activated by

(D and M) Average *Z* scored activity traces for each cluster classified by k-means clustering during D-glucose versus L-glucose (D, cluster X = 51%; cluster Y = 49%) or D-glucose versus lipid (M, cluster X = 36%; cluster Y = 64%) infusions. Cluster X (red) represents neurons inhibited by D-glucose; cluster Y (gray) represents non-responders or opposite responders.

(E and N) Summary of the proportions of CRF^{PVN} neurons significantly inhibited (blue; *Z* score < −1σ), activated (red; *Z* score > 1σ), or unaltered (gray) by ID infusion of D-glucose, L-glucose (E), or lipid (N). Lower panels quantify the proportion of L-glucose- or lipid-responsive neurons among D-glucose-inhibited cells.

(F and O) Scatter plots of individual *CRF*$^{PVN:GCaMP6}$ neuronal responses comparing *Z* scores for L-glucose (F) or lipid (O) on the y axis versus D-glucose response on the x axis. Dashed lines indicate ±1σ thresholds for responsiveness.

(G and P) Classification of neurons into four clusters based on response profiles: cluster 1: CRF^{PVN} neurons inhibited by D-glucose but stimulated by L-glucose or lipid (green), cluster 2: CRF^{PVN} neurons inhibited by D-glucose only (blue), cluster 3: CRF^{PVN} neurons stimulated by L-glucose or lipid only (red), and cluster 4: non-responsive CRF^{PVN} neurons (black).

(H and Q) Decoding performance of a time-evolving linear support vector machine (SVM) trained on calcium dynamics to distinguish between D-glucose and L-glucose (H) or D-glucose and lipid (Q) infusion sessions. Classifier accuracy using real data (black) is compared with shuffled data (gray).

(I and R) Mean decoding accuracy from classifiers trained on signals from each cluster separately or all clusters combined, compared with shuffled controls. Statistical significance was assessed using two-way ANOVA with Holm-Sidak correction. $^{**}p < 0.01$ and $^{****}p < 0.0001$.

(J and S) Histogram of tuning preference of individual CRF^{PVN} neurons for L-glucose versus D-glucose (I) or lipid versus D-glucose (R). Tuning preference: strength of cell's response preference for either stimulus. The tuning preference reflects the relative strength of neuronal activation between two stimuli, ranging from −1 (strong preference for D-glucose) to +1 (strong preference for L-glucose or lipid), with 0 indicating no preference.

See also Figure S3.

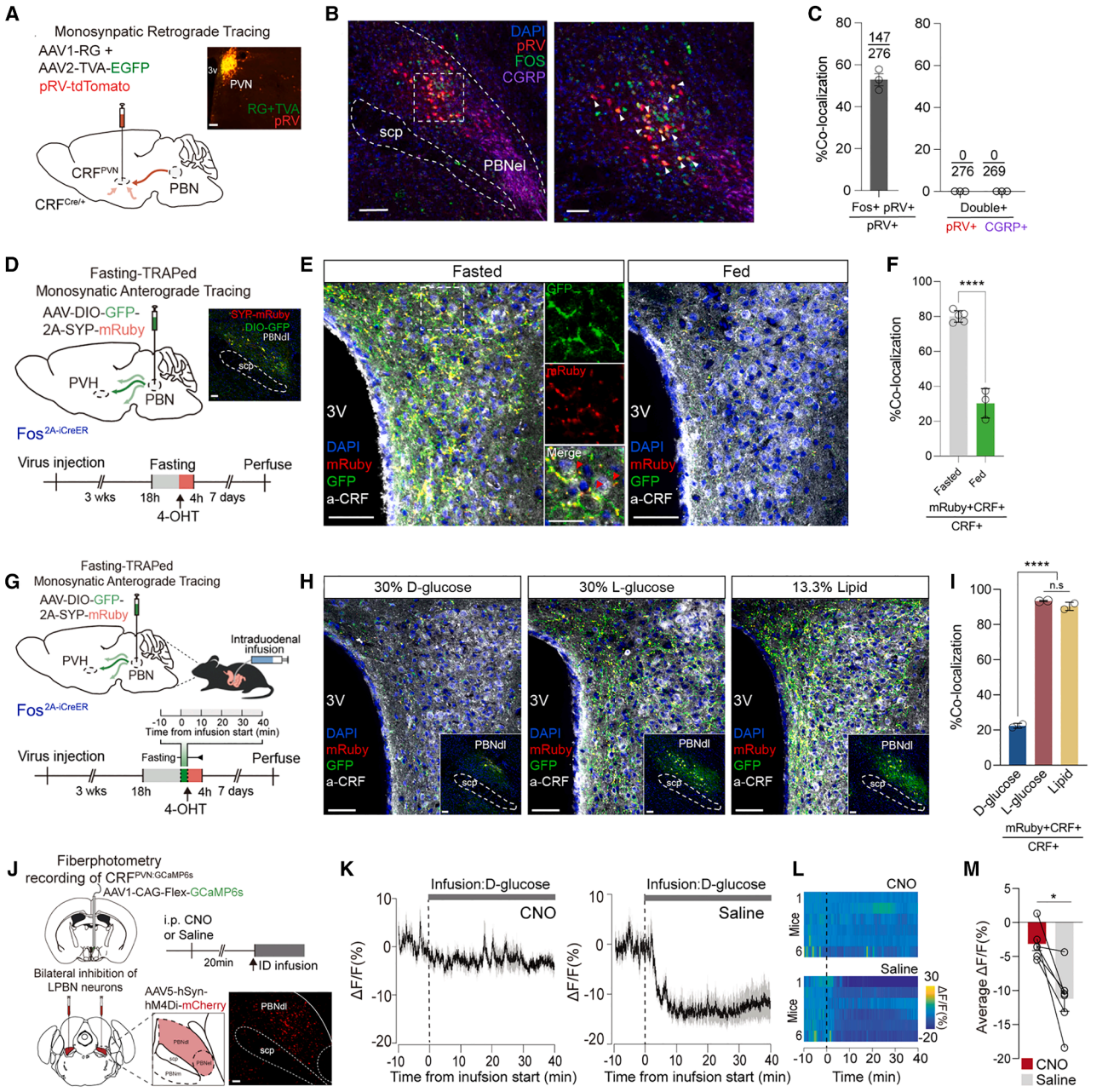

Figure 5. A subpopulation of PBNdl neurons relays intestinal D-glucose information to CRF^{PVN} neurons

(A) Schematic of monosynaptic retrograde tracing from CRF^{PVN} neurons using engineered rabies virus injected into the PVN of *Crf-IRES-Cre* mice. Right: representative image of the PVN showing the injection site with starter cells co-expressing RG+ avian glycoprotein EnvA receptor (TVA) (green) and rabies virus (RV) (red). Scale bar, 50 μm.

(B) Representative images illustrating retrogradely labeled cells (RV, red) in the PBNdl, co-stained with DAPI (blue), anti-CGRP (purple), and anti-cFOS (green) antibodies following 20 h of fasting. Magnified inset (white box) shows co-localization of cFOS and RV (yellow arrowheads). Scale bar, 50 μm.

(C) Quantification of RV-labeled PBNdl neurons co-expressing fasting-induced cFOS (left) or CGRP (right) (N = 3 mice).

(D) Schematic of monosynaptic anterograde tracing from fasting-TRAPed neurons in the PBNdl. Cre-dependent GFP-2A-synaptophysin-mRuby virus injected into the PBN of *Fos$^{2A\text{-}iCreER}$* mice. Right: representative confocal image GFP and mRuby expression in PBNdl neurons. Lower: Protocol showing targeted recombination in active populations (TRAP) induction by 4-OHT injection after 18 h of fasting. Scale bar: 50 μm.

(E) Representative confocal images showing the axonal terminals of fasting-TRAPed PBNdl neurons into the PVN, visualized by native GFP (green), mRuby (red), DAPI (blue), and CRF immunolabeling (white). Comparison is shown between 18-h fasted and fed conditions. Insets highlight single-channel images from the dotted box. Scale bar, 50 μm.

(legend continued on next page)

L-glucose (cluster X in Figure 4D). Classifying neurons based on dual responses revealed 19% fell into this bidirectional category (Figures 4F, 4G-green, and cluster 1in S3A). A support vector machine (SVM) trained with the calcium dynamics of CRF^{PVN} neurons from each cluster (clusters 1–4 in Figure 4G) distinguished D-glucose from L-glucose with higher accuracy. Notably, the decoder that was trained with CRF^{PVN} neurons in the bidirectional response group (cluster 1) showed significantly higher decoding accuracy compared with the decoders trained using CRF^{PVN} neurons from the other groups (Figure 4I and also see Figure 4H). Tuning analysis also identified 17.44% of CRF^{PVN} neurons as bidirectional responders (Figure 4J).

The ID infusion of isocaloric lipids significantly activated a large proportion of CRF^{PVN} neurons (Figures 4K, 4L, and 4N right; activated: 49%, inhibited: 1%, others: 50%; n = 80 cells), whereas protein had minimal effects (Figures S3C–S3E right; activated: 8%, inhibited: 9%, others: 83%; n = 149 cells), consistent with the results of fiber photometry. Approximately 56% of the D-glucose-inhibited CRF^{PVN} neurons were activated by lipids at the single-cell level (Figure 4N). K-means clustering and response classification revealed that 25% of CRF^{PVN} neurons were inhibited by D-glucose and activated by lipids (Figures 4M, cluster X, 4O, 4P green, and S3B, cluster 1). An SVM trained with CRF^{PVN} calcium dynamics in this bidirectional subpopulation achieved strong classification (Figures 4R and 4Q). Tuning analysis also showed that 30.98% of CRF^{PVN} neurons had this bidirectional profile (Figure 4S).

Additionally, a significant proportion of CRF^{PVN} neurons responded to D-fructose (Figures S3F–S3H right; activated: 33%, inhibited: 9%, n = 90 cells), with approximately 34% overlap with the D-glucose-inhibited CRF^{PVN} neurons. These results suggest the existence of a CRF^{PVN} subpopulation that responds bidirectionally to D-glucose and other nutrients, possibly aiding D-glucose recognition.

We next compared the dynamics of individual CRF^{PVN} neuronal activity during ID infusion of L-glucose, lipids, or D-fructose to determine whether the same CRF^{PVN} neurons were activated by all three stimuli at the single-cell level. Comparisons across infusions showed minimal overlap between neurons activated by L-glucose and lipids (Figures S3I and S3L). However, neurons responding to D-fructose were similar to those activated by L-glucose (Figures S3J and S3M) but distinct from lipid-responsive neurons (Figures S3K and S3N). Inferred from these findings, the D-glucose-inhibited CRF^{PVN} neuronal population bears subclusters that separately respond to L-glucose/D-fructose or to lipids, likely via distinct upstream inputs. Although single-cell imaging reveals these nutrient-specific subsets, lacking selective Cre drivers currently limits manipulation of these populations to study behavior.

A subpopulation of PBNdl neurons mediates D-glucose-evoked inhibition of CRF^{PVN} neurons

To identify upstream neurons conveying the duodenal D-glucose signal to CRF^{PVN} neurons, we conducted retrograde monosynaptic tracing using a modified pseudotyped rabies virus-avian virus envelope protein-glycoprotein-deleted-tdTomato (pRV-EnvA-dG-tdTomato) (Figure 5A). This revealed a subpopulation of the dorsal lateral parabrachial nucleus (PBNdl) neurons of the hindbrain that monosynaptically project to CRF^{PVN} neurons (Figure 5B). These traced neurons were distinct from CGRP-expressing PBNel neurons that primarily respond to aversive stimuli (Figures 5B and 5C).[48] Furthermore, a subset of PBNdl neurons that provide monosynaptic inputs to CRF^{PVN} neurons showed cFos activation induced after 18 h of fasting.

To validate the anatomical connections between the fasting-sensitive PBNdl neurons and CRF^{PVN} neurons, we anterogradely traced the PBNdl axonal projections to the PVN. To this end, we injected AAV1-hSyn-FLEx-mGFP-2A-Synaptophysin-mRuby into the PBNdl of $Fos^{2A\text{-}iCreER}$ mice and investigated whether fasting induces trapping of mGFP and synaptophysin-mRuby in the PBNdl axonal terminals that abut CRF^{PVN} neurons (Figure 5D). Following 18 h of fasting, the PBNdl afferent fibers in the PVN were exquisitely labeled with mGFP and synaptophysin-mRuby, closely apposed to CRF^{PVN} neurons, whereas fed mice showed minimal labeling (Figures 5E and 5F). These tracing and trapping results suggest that fasting selectively activates a subpopulation of PBNdl neurons that monosynaptically project to the PVN and that the PBNdl presynaptic terminals are in close proximity to CRF^{PVN} neurons, bearing possible synaptic connectivity with CRF^{PVN} neurons.

We next sought to determine whether the significant trapping of synaptophysin-mRuby and mGFP in the PBNdl afferents of fasted mice could be modulated by ID infusion of D-glucose or other macronutrients without orosensory stimulation (Figure 5G). Indeed, the ID infusion of D-glucose, but not nonnutritive

(F) Quantification of the percentage of CRF^{PVN} neurons surrounded by mRuby-labeled terminals under different conditions. One-way ANOVA test with multiple comparisons to shuffled data, $^{****}p < 0.0001$. Mean ± SEM.

(G) Schematic of monosynaptic anterograde tracing from fasting + ID infusion-TRAPed PBNdl neurons. Cre-dependent GFP-2A-synaptophysin-mRuby virus injected into the PBN of $Fos^{2A\text{-}iCreER}$ mice following ID infusion at the rate of 15 μL/min for 40 min.

(H) Representative images illustrating the axonal terminals of fasting + ID infusion-TRAPed PBNdl neurons into the PVN after 18-h fasted mice received ID infusion of 30% D-glucose, 30% L-glucose, or 13.3% intralipids. Insets depict the injection sites and starter cells in the PBN expressing GFP and mRuby. Scale bar, 50 μm (PVN) and 100 μm (PBN).

(I) Quantification of the percentage of CRF^{PVN} neurons surrounded by mRuby-positive terminals following different ID infusions. One-way ANOVA with multiple comparisons to shuffled data, $^{****}p < 0.0001$. Mean ± SEM.

(J) Schematic of dual viral injections for simultaneous manipulation and recording: AAV encoding Cre-dependent GCaMP6s injected into the PVN and AAV-hSyn-hM4Di-mCherry into the LPBN, permitting fiber photometry recording of $CRF^{PVN:GCaMP6}$ signals while chemogenetically silencing LPBN neurons. Protocol schematic shows i.p. injection of CNO or saline prior to nutrient ID infusion. Right: representative image of mCherry expression in the LPBN. Scale bar, 100 μm.

(K–M) PSTH plots (K), heatmaps (L), and quantifications (M) of ΔF/F(%) of $CRF^{PVN:GCaMP6}$ signals aligned to the onset of ID infusion of 30% D-glucose after CNO or saline administration. Paired Student's t test. $^{*}p < 0.05$. Mean ± SEM.

See also Figure S4.

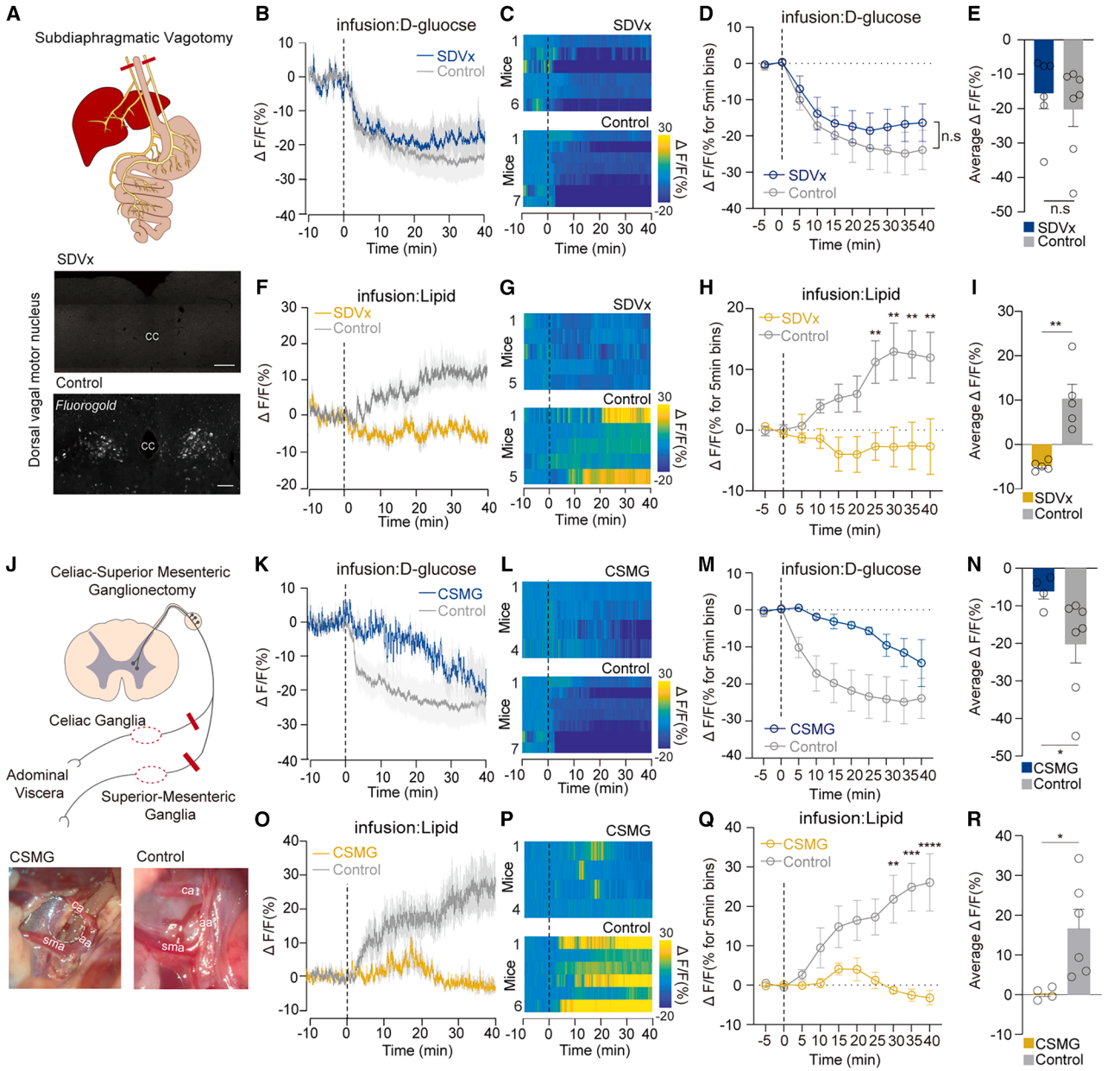

Figure 6. Distinct neural pathways convey intestinal nutrient signals to CRF^{PVN} neurons

(A) Schematic depicting the surgical procedure for total subdiaphragmatic vagotomy (SDVx) (upper). Representative images illustrating the histological verification using retrogradely traced fluorogold (white) in the dorsal motor nucleus of the vagus (DMV) in vagotomized (middle) and sham-operated control mice (below). Scale bars: 200 μm (middle) and 100 μm (bottom).

(B, C, F, and G) PSTH plots (B and F) and heatmaps (C and G) of ΔF/F(%) of *CRF*$^{PVN:GCaMP6}$ signals aligned to the onset of ID infusion of D-glucose (B and C) or lipid (F and G) in control (from Figure 1) and vagotomized mice (SDVx).

(D and H) Time-binned average ΔF/F(%) of *CRF*$^{PVN:GCaMP6}$ signals during 5-min intervals throughout ID infusion of D-glucose (D) or lipid (H) in control and SDVx mice.

(E and I) Quantification of ΔF/F(%) of *CRF*$^{PVN:GCaMP6}$ signals during ID infusion of D-glucose (E) or lipid (I) in control and SDVx mice.

(J) Schematic illustrating the surgical approach for celiac-superior mesenteric ganglionectomy (CSMGx) (upper). Representative images confirming successful removal of celiac ganglion (CG) and superior-mesenteric ganglion (SMG) in CSMGx mice versus intact ganglion in sham controls (lower). Anatomical landmarks include the celiac artery (ca), superior-mesenteric artery (sma), and aorta (aa).

(K, L, O, and P) PSTH plots (K and O) and heatmaps (L and P) of ΔF/F(%) of *CRF*$^{PVN:GCaMP6}$ signals aligned to ID infusion of D-glucose (K and L) or lipid (O and P) in fasted control and CSMGx mice.

(legend continued on next page)

L-glucose or isocaloric lipids, significantly reduced the fasting-induced trapping of synaptophysin-mRuby and mGFP in the PBNdl afferents that innervate CRF^{PVN} neurons (Figures 5H and 5I). Inferred from these findings, we propose that the fasting-activated PBNdl neurons, which are inhibited by duodenal D-glucose and are mostly glutamatergic,[49] provide an inhibitory input to CRF^{PVN} neurons.

To assess whether these PBNdl neurons are functionally important for the gut-glucose-induced inhibition of CRF^{PVN} neurons, we monitored the CRF^{PVN} neuronal response to ID infusion of D-glucose during chemogenetic silencing. Mice that had received the bilateral PBNdl injections of AAV-hSyn-hM4Di-mCherry received an i.p. injection of CNO or saline 20 min before initiating ID infusion of D-glucose under fasting (Figure 5J). Control fasted mice not expressing hM4Di were unaffected by CNO (Figures S4A–S4E). Notably, chemogenetic silencing of PBNdl neurons with CNO abolished D-glucose-induced inhibition of CRF^{PVN} neurons compared with saline-injected controls (Figures 5K–5M). However, silencing did not affect CRF^{PVN} neuronal responses to L-glucose, lipids, or the i.p. injection of LiCl, which caused gastric malaise or visceral pain[50] and resulted in activation of CRF^{PVN} neurons[24] (Figures S4F–S4Q). These findings suggest that the PBNdl neurons selectively mediate the D-glucose-induced inhibition of CRF^{PVN} neuronal activity.

The gut-brain axis mediates the nutrient-evoked CRF^{PVN} neuronal response

We next sought to determine the contribution of the vagal or spinal neural pathway to the conveyance of nutrient-related signals from the gut to CRF^{PVN} neurons. We began by performing a total subdiaphragmatic vagotomy (SDVx) in mice that had been fitted with an ID catheter to facilitate duodenal nutrient infusions; this surgical transection of the vagus nerve severed all vagal sensory axons that course from the duodenum to the brainstem.[51] We then measured the CRF^{PVN} neuronal response to a duodenal infusion of sugar or lipids (Figure 6A). The success of the SDVx was confirmed by the absence of retrograde tracer, fluorogold, within the dorsal motor nucleus of the vagus nerve following i.p. injection of fluorogold (Figure 6A lower). We observed that SDVx did not block the acute inhibitory effects of ID-infused D-glucose or sucrose on the CRF^{PVN} neuronal response (Figures 6B–6E and S5A–S5D). By contrast, SDVx significantly attenuated the excitatory response of CRF^{PVN} neurons to the ID infusion of lipids (Figures 6F–6I and S5E–S5H). Moreover, the increase in CRF^{PVN} neuronal activity by nonnutritive L-glucose was also blunted in vagotomized mice (Figures S5I–S5P).

Because neither humoral nor vagal signaling appeared to be recruited for duodenal D-glucose to communicate with CRF^{PVN} neurons, we extended our investigation to evaluate the impact of non-vagal splanchnic afferents, which innervate the abdominal viscera.[52] Specifically, we removed the celiac superior mesenteric ganglion (CSMGx) through which the splanchnic nerves pass from the intestine to the brain[52] (Figure 6J). Removal of the CSMG significantly attenuated the ability of duodenal D-glucose to rapidly reduce CRF^{PVN} neuronal activity (Figures 6K–6N). CSMGx also blocked the activation of CRF^{PVN} neuronal activity by the ID infusion of lipids (Figures 6O–6R). However, CSMGx did not impede the L-glucose-induced stimulation of CRF^{PVN} neuronal activity (Figures S5Q–S5T). Taken together, these results demonstrate that the CRF^{PVN} neuronal response to post-absorptive D-glucose signal requires the spinal pathway; by contrast, CRF^{PVN} neuronal response to the ID infusion of L-glucose requires the vagal pathway, while the CRF^{PVN} response to infused lipids requires either the spinal or vagal pathway.

PBNdl neurons receive the monosynaptic input from spinal nerves

Having shown that the D-glucose-induced inhibition of CRF^{PVN} neuronal activity requires non-vagal splanchnic afferents and PBNdl neurons, and that CRF^{PVN} neurons receive the monosynaptic input from PBNdl neurons that were activated by fasting, we next sought to determine whether the fasting-sensitive PBNdl neurons are coupled selectively to the non-vagal splanchnic afferents from the spinal cord. To this end, we conducted retrograde tracing of the monosynaptic inputs to the fasting-sensitive PBNdl neurons using an engineered rabies virus. We co-injected an engineered monosynaptic rabies virus (EnvA pseudotyped rabies virus-mCherry) and AAVs expressing helper constructs (AAV2/1-hS-FLEX-TVA-HA-N2cG) into the PBNdl of $Fos^{2A\text{-}iCreER}$ mice, in which the expression of cre^{ER} was induced by fasting for 18 h, and determined whether fasting induces trapping of mCherry in a spinal nerve, a vagal nerve, or both (Figure 7A). We confirmed the labeling of starter cells in the PBNdl following a period of fasting (Figure 7B). By performing 2D and 3D histological analyses of the spinal cord and the nodose ganglion, we identified a distinct population of the spinal nerve with cell bodies located in the lumbar and thoracic regions of the spinal cord, which project extensively in a rostral direction, whereas we did not detect any labeling of rabies-derived mCherry in the vagus nerve in the nodose ganglion (Figures 7C–7E; Video S1). These findings suggest that the fasting-sensitive PBNdl neuronal subpopulation receives monosynaptic inputs from the spinal pathway.

DISCUSSION

The HPA axis in mammals, which is regulated by upstream CRF^{PVN} neurons and CRF peptide, mediates several stress responses, one of which is to maintain glucose homeostasis during periods of fasting. The neuroendocrine regulation of CRF^{PVN} neurons through the HPA axis is implicated in the CRR, which

(M and Q) Time-binned average ΔF/F(%) of $CRF^{PVN:GCaMP6}$ signals during 5-min intervals throughout ID infusion of D-glucose (M) or lipid (Q) in fasted control and CSMGx mice.
(N and R) Quantification of ΔF/F(%) of $CRF^{PVN:GCaMP6}$ signals during ID infusion of D-glucose (N) or lipid (R) in fasted control and CSMGx mice.
$^{*}p < 0.05$, $^{**}p < 0.01$, $^{***}p < 0.001$, and $^{****}p < 0.0001$. n.s., non-significant. Mean ± SEM.
See also Figures S2 and S5.

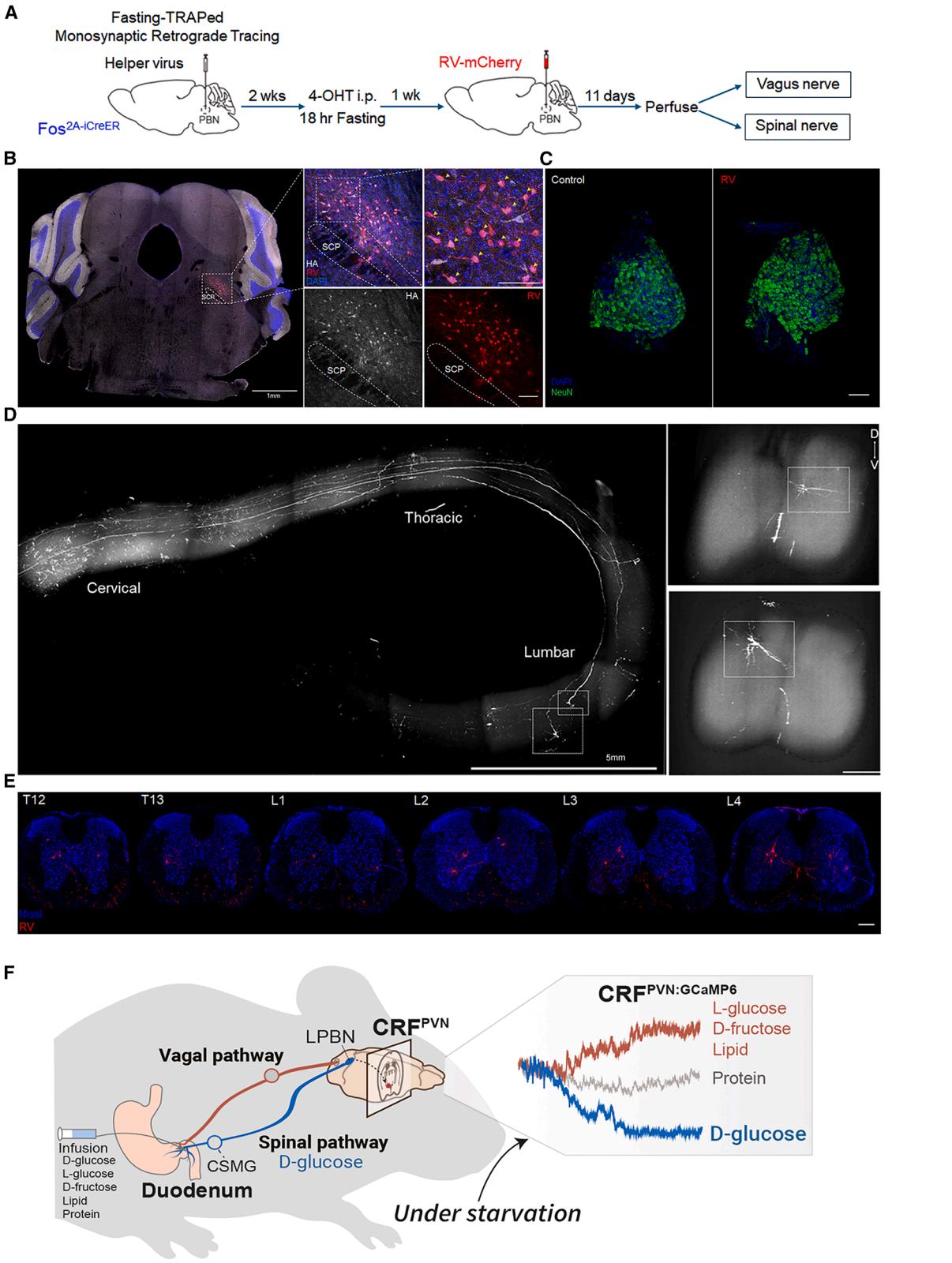

(legend on next page)

results in the synthesis and release of glucocorticoid from the adrenal gland and eventually increases circulating glucose levels in fasted animals.[53] Our findings show that in addition to their neuroendocrine role in CRR-directed glucose homeostasis, CRF^{PVN} neurons respond rapidly to an intestinal infusion of D-glucose and motivate its consumption, particularly under fasted conditions. It is unclear, however, how CRF^{PVN} neurons engage distinct downstream pathways for (1) the slow and sustained release of hormones and (2) the rapid regulation of behavior to achieve glucose homeostasis. A large proportion of CRF^{PVN} neurons is stimulated by fasting, when the production and secretion of CRF peptides that stimulate the HPA axis for the CRR-directed glucose homeostasis is enhanced.[24,53] By contrast, the results of *CRF* conditional knockout and bilateral adrenalectomy experiments suggest that the rapid physiological and behavioral responses of CRF^{PVN} neurons to the intestinal infusion of D-glucose do not require *CRF* or activation of the HPA axis (Figures S2H–S2K). Rather, the CRF peptide or the HPA axis may not be important for the CRF^{PVN} neuronal subpopulation to respond rapidly and encode D-glucose. Nonetheless, the inhibition of CRF^{PVN} neuronal activity and CRF peptide secretion induced by intestinal D-glucose would mitigate the fasting-induced activation of the HPA axis.

Animals in the wild often experience the sensation of hunger, which is highly stressful and could stimulate CRF^{PVN} neuronal activity. Indeed, the fasting-induced activation of CRF neurons enhanced the activity of the HPA axis and increased plasma corticosterone levels[21]; conversely, the suppression of CRF^{PVN} neurons would lower plasma corticosterone. Severe food deprivation drives rodents to prioritize dietary sugar over other macronutrients,[54,55] likely due to the rapid ability of sugar—particularly D-glucose—to replenish the deprived energy reservoir and fuel brain cells. This increased preference for D-glucose-containing foods provides a survival advantage. Indeed, a study has shown that a subset of CRF^{PVN} neurons plays a crucial role in guiding the dietary selection of carbohydrates over fat during fasting.[56] Because D-glucose is particularly effective in alleviating the fasting-induced stress, it may be advantageous to recruit a component of the stress circuit as a D-glucose encoder. This mechanism would link intestinal D-glucose detection to the inhibition of the HPA axis, thereby contributing to glucose homeostasis. By contrast, other macronutrients and even other nutritive sugars like D-fructose that are not readily converted into brain fuel stimulated the activity of CRF^{PVN} neurons, linking the intake of these less desirable nutrients to an enhanced HPA stress response. Moreover, the presence of opposing effects—wherein the system exhibits the opposite responses to D-glucose versus lipid or D-fructose—may enhance its ability to distinguish between rapidly metabolizable glucose and nutrients that provide energy in a less immediately accessible form.

The vagal and spinal pathways have been implicated as key gut-brain neural pathways for mediating a rapid response by CNS neurons to nutrients infused in the gastrointestinal tract.[52] Which neural pathway is important for the behavioral and physiological responses to infused D-glucose or D-glucose-containing sugar remains unclear, however.[8,33,57,58] Our fiber photometry recordings, combined with CSMGx, demonstrate that the rapid inhibition of CRF^{PVN} neuronal activity induced by D-glucose requires the spinal pathway (Figures 6K–6N). This finding is consistent with the spinal-dependent D-glucose–induced inhibition of AgRP neurons[8] and the role of spinal afferents in the hypoglycemia-dependent CRR.[59,60] Consistent with these findings, monosynaptic retrograde tracing experiments revealed that fasting-sensitive PBNdl neurons, which provide presynaptic input to CRF^{PVN} neurons, are anatomically connected to a subset of the spinal neurons with cell bodies distally located in the thoracic and lumbar segments of the spinal cord (Figures 7A–7E). *Drosophila* DH44 neurons in the brain receive information about glucose levels in the body through glucose-sensing neurons in the spinal nerve of the ventral nerve cord, which connects the body to the brain and is considered analogous to the mammalian spinal cord.[19] The finding that the D-glucose-specific CRF^{PVN} neuronal response required the activity of the spinal pathway may suggest a functional conservation of the pathway leading to the mammalian CRF^{PVN} and *Drosophila* DH44 neurons in regulating the sugar-specific appetite during fasting.

The dorsolateral region of the PBN (PBNdl) appeared to represent a neural population that functions as an intermediate node to convey the signal of intestinal glucose to CRF^{PVN} neurons during fasting. Monosynaptic tracing revealed that CRF^{PVN} neurons

Figure 7. Monosynaptic retrograde tracing from PBNdl neurons reveals spinal neurons

(A) Schematic illustrating the monosynaptic retrograde tracing approach targeting PBNdl neurons. Engineered rabies virus (RV) was injected into the PBNdl of $Fos^{2A\text{-}iCreER}$ mice to selectively label presynaptic inputs.

(B) Representative images of coronal brain sections showing RV-labeled neurons (white dotted box) in the PBN (left). Higher-magnification images showing starter cells in the PBNdl expressing RV-mCherry and/or HA tag (middle upper). Further magnified view of the white box revealing double-positive starter cells (yellow arrowheads) stained with DAPI (blue) (right upper). Separate channels illustrating HA-only (middle lower) and mCherry (right lower) fluorescence in the PBN. Scale bar, 100 μm.

(C) Representative images of the jugular-nodose ganglion from control (left) and experimental (right) mice following RV-mCherry injection, co-stained with anti-NeuN (green) and DAPI (blue). Scale bar, 100 μm.

(D) Whole-mount cleared spinal cord imaged using a light-sheet microscope. 3D rendering of the entire spinal cord (left). High-magnification optical slices from thoracic and lumbar regions (white boxes) showing detailed RV labeling (right). Scale bars, 500 μm.

(E) Representative coronal sections of the thoracic and lumbar spinal cord showing RV-mCherry-labeled neurons (red) and Nissl staining (blue). Scale bars, 200 μm.

(F) Proposed working model illustrating the neural circuitry linking intestinal D-glucose sensing to CRF^{PVN} neuronal activity. During fasting, ID D-glucose infusion selectively suppresses this activity via a spinal nerve-mediated pathway that inhibits fasting-sensitive PBNdl neurons. By contrast, other nutrients (e.g., L-glucose and lipids) activate CRF^{+}PVN neurons via vagal and/or spinal pathways, independently of fasting-sensitive PBNdl neurons.

See also Video S1.

received inputs from various brain regions, including the PBN (Figure 5A).[28] D-glucose–induced inhibition of CRF^{PVN} neuronal activity in fasted mice was blocked by the chemogenetic silencing of PBNdl neurons (Figures 5J–5M). The PBN area, which is located in the pons, is known to relay a wide range of sensory information—including the sensation of taste, mechanosensation, and pain—and send multiple projections to regions in the forebrain.[61–63] The PBN is also involved in a wide range of visceral interoception activities through both spinal and vagal afferents.[64–66] The PBN neurons receive input from both peripheral vagal signals (through monosynaptic input from the nucleus tractus solitarius)[67] and directly from the dorsal laminae of the spinal cord.[68,69] Furthermore, it has been suggested that different subpopulations of PBN neurons encode both aversive and rewarding interoceptive signals from the gut. Calcitonin gene-related peptide (CGRP) neurons in the externolateral regions of the PBN, for example, responded to aversive stimuli, such as visceral malaise, by suppressing feeding activity, whereas PBNdl neurons responded to the gut-induced reward.[66,70,71] Our results show that a subpopulation of PBNdl neurons, which monosynaptically projects to CRF^{PVN} neurons, is distributed to dorsolateral regions of the PBN (being largely excluded from $CGRP^{PBN}$ neurons) and activated by fasting (Figures 5D–5F). Intriguingly, the fasting-induced activation of the PBNdl subpopulation was suppressed by the ID infusion of D-glucose but not by L-glucose or lipids (Figures 5G–5I). Given that the majority of PBN neurons are glutamatergic,[49] it is conceivable that the signal representing duodenal D-glucose that is transmitted through the spinal gut-brain pathway inhibits the fasting-activated PBNdl neurons, which stimulate CRF^{PVN} neurons and ultimately inhibit the activity of CRF^{PVN} neurons (see Figure 7F). Molecularly defining the fasting-activated PBNdl neurons could provide deeper insight into how gut-derived signals shape CRF^{PVN} neuronal activity in the future.

RESOURCE AVAILABILITY

Lead contact

Further information and requests for resources and reagents should be directed to the lead contact, Greg S.B. Suh (seongbaesuh@kaist.ac.kr).

Materials availability

All the original reagents presented in this study are available from the lead contact on a reasonable request.

Data and code availability

- All raw data generated in this study are presented in Table S2. All data reported in this paper will be shared by the lead contact upon request. The codes and software used in the study have been deposited at https://doi.org/10.5281/zenodo.15392507.
- Any additional information required to reanalyze the data reported in this paper is available from the lead contact upon request.

ACKNOWLEDGMENTS

We thank J.W. Sohn, D. Lin, and I. de Araujo for the helpful discussions and initial assistance with this work; S.H. Park for his assistance with optogenetic experiments; the laboratory of the late Wylie Vale for providing an aliquot of anti-CRF antibody; Daye Kim for her assistance in acquiring holistic images from the spinal cord; Y.H. Song and D. Jeong for their assistance with rabies viral tracing; I.S. Choi for his assistance with two-photon imaging; and M. Jin, K. Kuchibhotla, H. Lu, E.S. Papadoyannis, E.X. Morina, and C. Verducci for their assistance with behavioral studies. We thank the members of the Suh laboratory for stimulating discussion and comments on the paper. This work is supported by the TJ Park Science Fellowship, the ASAN Biomedical Science Fellowship, and the KAIST Advanced Institute for Science-X research fellowship to J.K.; a Pew Innovation Fund to R.C.F.; the Institute for Basic Science (IBS-R002-A2) to S.-H.L.; the KAIST Chancellor's Fund; and grants from the Samsung Science and Technology Foundation (project number: SSTF-BA-1802-11) and the National Research Foundation of Korea (NRF-2021M3F3A2A01037365, NRF-2022M3A9F3082982, RS-2023-00255126, and RS-2024-00467213-Boston-Korea Project) to G.S.B.S.

AUTHOR CONTRIBUTIONS

J.K., Shinhye Kim, and W.J. performed nearly all experiments and produced figures. Y.K. assisted with a fiber photometry experiment. J.K. and W.J. performed and analyzed two-photon experiments with assistance from H.-Y.P. in S.-H.L.'s lab. Sehun Kim and Y.-G.P. performed clearing and imaging of the spinal cord. D.Y.Y. and I.K.H. helped with adrenalectomy surgery. S.-H.L. and G.J.S. helped with ID infusion, SDVx, and CSMGx. J.K., Shinhye Kim, W.J., and G.S.B.S. analyzed and discussed the results. J.K., Shinhye Kim, W.J., and G.S.B.S. wrote the manuscript with inputs from other authors. G.S.B.S. supervised the project.

DECLARATION OF INTERESTS

The authors declare no competing interests.

STAR★METHODS

Detailed methods are provided in the online version of this paper and include the following:

SUPPLEMENTAL INFORMATION

Supplemental information can be found online at https://doi.org/10.1016/j.neuron.2025.05.024.

Received: June 11, 2024
Revised: March 14, 2025
Accepted: May 22, 2025
Published: June 20, 2025

REFERENCES

1. Mergenthaler, P., Lindauer, U., Dienel, G.A., and Meisel, A. (2013). Sugar for the brain: the role of glucose in physiological and pathological brain function. Trends Neurosci. *36*, 587–597. https://doi.org/10.1016/j.tins.2013.07.001.
2. Kety, S.S. (1957). The general metabolism of the brain in vivo. In Metabolism of the Nervous System (Elsevier), pp. 221–237. https://doi.org/10.1016/B978-0-08-009062-7.50026-6.
3. Ritter, S. (2017). Monitoring and maintenance of brain glucose supply: Importance of hindbrain catecholamine neurons in this multifaceted task. In Appetite and Food Intake, R.B.S. Harris, ed. (CRC Press), pp. 177–204. https://doi.org/10.1201/9781315120171-9.
4. Fournel, A., Marlin, A., Abot, A., Pasquio, C., Cirillo, C., Cani, P.D., and Knauf, C. (2016). Glucosensing in the gastrointestinal tract: Impact on glucose metabolism. Am. J. Physiol. Gastrointest. Liver Physiol. *310*, G645–G658. https://doi.org/10.1152/ajpgi.00015.2016.
5. Beutler, L.R., Chen, Y., Ahn, J.S., Lin, Y.C., Essner, R.A., and Knight, Z.A. (2017). Dynamics of Gut-Brain Communication Underlying Hunger. Neuron *96*, 461–475. https://doi.org/10.1016/j.neuron.2017.09.043.
6. Su, Z., Alhadeff, A.L., and Betley, J.N. (2017). Nutritive, post-ingestive signals are the primary regulators of AgRP neuron activity. Cell Rep. *21*, 2724–2736. https://doi.org/10.1016/j.celrep.2017.11.036.
7. Alhadeff, A.L., Goldstein, N., Park, O., Klima, M.L., Vargas, A., and Betley, J.N. (2019). Natural and drug rewards engage distinct pathways that converge on coordinated hypothalamic and reward circuits. Neuron *103*, 891–908. https://doi.org/10.1016/j.neuron.2019.05.050.
8. Goldstein, N., McKnight, A.D., Carty, J.R.E., Arnold, M., Betley, J.N., and Alhadeff, A.L. (2021). Hypothalamic detection of macronutrients via multiple gut-brain pathways. Cell Metab. *33*, 676–687. https://doi.org/10.1016/j.cmet.2020.12.018.
9. Nelson, G., Hoon, M.A., Chandrashekar, J., Zhang, Y., Ryba, N.J., and Zuker, C.S. (2001). Mammalian sweet taste receptors. Cell *106*, 381–390. https://doi.org/10.1016/s0092-8674(01)00451-2.
10. Spector, A.C., and Travers, S.P. (2005). The representation of taste quality in the mammalian nervous system. Behav. Cogn. Neurosci. Rev. *4*, 143–191. https://doi.org/10.1177/1534582305280031.
11. de Araujo, I.E., Oliveira-Maia, A.J., Sotnikova, T.D., Gainetdinov, R.R., Caron, M.G., Nicolelis, M.A.L., and Simon, S.A. (2008). Food reward in the absence of taste receptor signaling. Neuron *57*, 930–941. https://doi.org/10.1016/j.neuron.2008.01.032.
12. Holman, G.L. (1969). Intragastric reinforcement effect. J. Comp. Physiol. Psychol. *69*, 432–441. https://doi.org/10.1037/h0028233.
13. Sclafani, A. (2001). Post-ingestive positive controls of ingestive behavior. Appetite *36*, 79–83. https://doi.org/10.1006/appe.2000.0370.
14. Sclafani, A., and Ackroff, K. (2016). Operant licking for intragastric sugar infusions: Differential reinforcing actions of glucose, sucrose and fructose in mice. Physiol. Behav. *153*, 115–124. https://doi.org/10.1016/j.physbeh.2015.10.021.
15. Tellez, L.A., Han, W., Zhang, X., Ferreira, T.L., Perez, I.O., Shammah-Lagnado, S.J., van den Pol, A.N., and de Araujo, I.E. (2016). Separate circuitries encode the hedonic and nutritional values of sugar. Nat. Neurosci. *19*, 465–470. https://doi.org/10.1038/nn.4224.
16. Dus, M., Min, S., Keene, A.C., Lee, G.Y., and Suh, G.S.B. (2011). Taste-independent detection of the caloric content of sugar in Drosophila. Proc. Natl. Acad. Sci. USA *108*, 11644–11649. https://doi.org/10.1073/pnas.1017096108.
17. Dus, M., Ai, M., and Suh, G.S.B. (2013). Taste-independent nutrient selection is mediated by a brain-specific Na+ /solute co-transporter in Drosophila. Nat. Neurosci. *16*, 526–528. https://doi.org/10.1038/nn.3372.
18. Dus, M., Lai, J.S.-Y., Gunapala, K.M., Min, S., Tayler, T.D., Hergarden, A.C., Geraud, E., Joseph, C.M., and Suh, G.S.B. (2015). Nutrient sensor in the brain directs the action of the brain-gut axis in Drosophila. Neuron *87*, 139–151. https://doi.org/10.1016/j.neuron.2015.05.032.
19. Oh, Y., Lai, J.S.Y., Min, S., Huang, H.W., Liberles, S.D., Ryoo, H.D., and Suh, G.S.B. (2021). Periphery signals generated by Piezo-mediated stomach stretch and Neuromedin-mediated glucose load regulate the Drosophila brain nutrient sensor. Neuron *109*, 1979–1995. https://doi.org/10.1016/j.neuron.2021.04.028.
20. Lovejoy, D.A., and Jahan, S. (2006). Phylogeny of the corticotropin-releasing factor family of peptides in the metazoa. Gen. Comp. Endocrinol. *146*, 1–8. https://doi.org/10.1016/j.ygcen.2005.11.019.
21. Smith, S.M., and Vale, W.W. (2006). The role of the hypothalamic-pituitary-adrenal axis in neuroendocrine responses to stress. Dial. Clin. Neurosci. *8*, 383–395. https://doi.org/10.31887/DCNS.2006.8.4/ssmith.
22. Baxter, J.D. (1976). Glucocorticoid hormone action. Pharmacol. Ther. B *2*, 605–669. https://doi.org/10.1016/0306-039x(76)90010-6.
23. Füzesi, T., Daviu, N., Wamsteeker Cusulin, J.I.W., Bonin, R.P., and Bains, J.S. (2016). Hypothalamic CRH neurons orchestrate complex behaviours after stress. Nat. Commun. *7*, 11937. https://doi.org/10.1038/ncomms11937.
24. Kim, J., Lee, S., Fang, Y.Y., Shin, A., Park, S., Hashikawa, K., Bhat, S., Kim, D., Sohn, J.W., Lin, D., et al. (2019). Rapid, biphasic CRF neuronal responses encode positive and negative valence. Nat. Neurosci. *22*, 576–585. https://doi.org/10.1038/s41593-019-0342-2.
25. Daviu, N., Füzesi, T., Rosenegger, D.G., Rasiah, N.P., Sterley, T.L., Peringod, G., and Bains, J.S. (2020). Paraventricular nucleus CRH neurons encode stress controllability and regulate defensive behavior selection. Nat. Neurosci. *23*, 398–410. https://doi.org/10.1038/s41593-020-0591-0.
26. Wu, W.-L., Adame, M.D., Liou, C.-W., Barlow, J.T., Lai, T.-T., Sharon, G., Schretter, C.E., Needham, B.D., Wang, M.I., Tang, W., et al. (2021). Microbiota regulate social behaviour via stress response neurons in the brain. Nature *595*, 409–414. https://doi.org/10.1038/s41586-021-03669-y.
27. Yuan, Y., Wu, W., Chen, M., Cai, F., Fan, C., Shen, W., Sun, W., and Hu, J. (2019). Reward Inhibits Paraventricular CRH Neurons to Relieve Stress. Curr. Biol. *29*, 1243–1251. https://doi.org/10.1016/j.cub.2019.02.048.
28. Lee, E.J., Hanchate, N.K., Kondoh, K., Tong, A.P.S., Kuang, D., Spray, A., Ye, X., and Buck, L.B. (2020). A psychological stressor conveyed by appetite-linked neurons. Sci. Adv. *6*, eaay5366. https://doi.org/10.1126/sciadv.aay5366.
29. Wang, P.Y.T., Caspi, L., Lam, C.K.L., Chari, M., Li, X., Light, P.E., Gutierrez-Juarez, R., Ang, M., Schwartz, G.J., and Lam, T.K.T. (2008). Upper intestinal lipids trigger a gut-brain-liver axis to regulate glucose production. Nature *452*, 1012–1016. https://doi.org/10.1038/nature06852.
30. Han, W., T.L, Perkins, M.H., Perez, I.O., Qu, T., Ferreira, J., Ferreira, T.L., Quinn, D., Liu, Z.W., Gao, X.B., et al. (2018). A Neural Circuit for Gut-Induced Reward. Cell *175*, 665–678. https://doi.org/10.1016/j.cell.2018.08.049.
31. Duca, F.A., Waise, T.M.Z., Peppler, W.T., and Lam, T.K.T. (2021). The metabolic impact of small intestinal nutrient sensing. Nat. Commun. *12*, 903. https://doi.org/10.1038/s41467-021-21235-y.
32. Magnuson, B.A., Carakostas, M.C., Moore, N.H., Poulos, S.P., and Renwick, A.G. (2016). Biological fate of low-calorie sweeteners. Nutr. Rev. *74*, 670–689. https://doi.org/10.1093/nutrit/nuw032.
33. Tan, H.E., Sisti, A.C., Jin, H., Vignovich, M., Villavicencio, M., Tsang, K.S., Goffer, Y., and Zuker, C.S. (2020). The gut-brain axis mediates sugar preference. Nature *580*, 511–516. https://doi.org/10.1038/s41586-020-2199-7.

34. Betz, A.L., Drewes, L.R., and Gilboe, D.D. (1975). Inhibition of glucose transport into brain by phlorizin, phloretin and glucose analogues. Biochim. Biophys. Acta *406*, 505–515. https://doi.org/10.1016/0005-2736(75)90028-0.

35. Gorboulev, V., Schürmann, A., Vallon, V., Kipp, H., Jaschke, A., Klessen, D., Friedrich, A., Scherneck, S., Rieg, T., Cunard, R., et al. (2012). Na(+)-D-glucose cotransporter SGLT1 is pivotal for intestinal glucose absorption and glucose-dependent incretin secretion. Diabetes *61*, 187–196. https://doi.org/10.2337/db11-1029.

36. Röder, P.V., Geillinger, K.E., Zietek, T.S., Thorens, B., Koepsell, H., and Daniel, H. (2014). The role of SGLT1 and GLUT2 in intestinal glucose transport and sensing. PLoS One *9*, e89977. https://doi.org/10.1371/journal.pone.0089977.

37. Schwartz, G.J., and Zeltser, L.M. (2013). Functional organization of neuronal and humoral signals regulating feeding behavior. Annu. Rev. Nutr. *33*, 1–21. https://doi.org/10.1146/annurev-nutr-071812-161125.

38. Lu, V.B., Gribble, F.M., and Reimann, F. (2021). Nutrient-Induced Cellular Mechanisms of Gut Hormone Secretion. Nutrients *13*, 883. https://doi.org/10.3390/nu13030883.

39. Ferreira, J.G., Tellez, L.A., Ren, X., Yeckel, C.W., and de Araujo, I.E. (2012). Regulation of fat intake in the absence of flavour signalling. J. Physiol. *590*, 953–972. https://doi.org/10.1113/jphysiol.2011.218289.

40. Domingos, A.I., Vaynshteyn, J., Voss, H.U., Ren, X., Gradinaru, V., Zang, F., Deisseroth, K., de Araujo, I.E., and Friedman, J. (2011). Leptin regulates the reward value of nutrient. Nat. Neurosci. *14*, 1562–1568. https://doi.org/10.1038/nn.2977.

41. Buch, T., Heppner, F.L., Tertilt, C., Heinen, T.J.A.J., Kremer, M., Wunderlich, F.T., Jung, S., and Waisman, A. (2005). A Cre-inducible diphtheria toxin receptor mediates cell lineage ablation after toxin administration. Nat. Methods *2*, 419–426. https://doi.org/10.1038/nmeth762.

42. Garfield, A.S., Li, C., Madara, J.C., Shah, B.P., Webber, E., Steger, J.S., Campbell, J.N., Gavrilova, O., Lee, C.E., Olson, D.P., et al. (2015). A neural basis for melanocortin-4 receptor-regulated appetite. Nat. Neurosci. *18*, 863–871. https://doi.org/10.1038/nn.4011.

43. Li, C., Navarrete, J., Liang-Guallpa, J., Lu, C., Funderburk, S.C., Chang, R. B., Liberles, S.D., Olson, D.P., and Krashes, M.J. (2019). Defined paraventricular hypothalamic populations exhibit differential responses to food contingent on caloric state. Cell Metab. *29*, 681–694. https://doi.org/10.1016/j.cmet.2018.10.016.

44. Vale, W., Spiess, J., Rivier, C., and Rivier, J. (1981). Characterization of a 41-residue ovine hypothalamic peptide that stimulates secretion of corticotropin and beta-endorphin. Science *213*, 1394–1397. https://doi.org/10.1126/science.6267699.

45. Ulrich-Lai, Y.M., and Herman, J.P. (2009). Neural regulation of endocrine and autonomic stress responses. Nat. Rev. Neurosci. *10*, 397–409. https://doi.org/10.1038/nrn2647.

46. Zhang, R., Asai, M., Mahoney, C.E., Joachim, M., Shen, Y., Gunner, G., and Majzoub, J.A. (2017). Loss of hypothalamic corticotropin-releasing hormone markedly reduces anxiety behaviors in mice. Mol. Psychiatry *22*, 733–744. https://doi.org/10.1038/mp.2016.136.

47. Bhatnagar, S., Bell, M.E., Liang, J., Soriano, L., Nagy, T.R., and Dallman, M.F. (2000). Corticosterone facilitates saccharin intake in adrenalectomized rats: does corticosterone increase stimulus salience? J. Neuroendocrinol. *12*, 453–460. https://doi.org/10.1046/j.1365-2826.2000.00487.x.

48. Campos, C.A., Bowen, A.J., Roman, C.W., and Palmiter, R.D. (2018). Encoding of danger by parabrachial CGRP neurons. Nature *555*, 617–622. https://doi.org/10.1038/nature25511.

49. Pauli, J.L., Chen, J.Y., Basiri, M.L., Park, S., Carter, M.E., Sanz, E., McKnight, G.S., Stuber, G.D., and Palmiter, R.D. (2022). Molecular and anatomical characterization of parabrachial neurons and their axonal projections. eLife *11*, e81868. https://doi.org/10.7554/eLife.81868.

50. Meachum, C.L., and Bernstein, I.L. (1992). Behavioral conditioned responses to contextual and odor stimuli paired with LiCl administration. Physiol. Behav. *52*, 895–899. https://doi.org/10.1016/0031-9384(92)90368-c.

51. Schwartz, G.J. (2000). The role of gastrointestinal vagal afferents in the control of food intake: current prospects. Nutrition *16*, 866–873. https://doi.org/10.1016/s0899-9007(00)00464-0.

52. Sclafani, A., Ackroff, K., and Schwartz, G.J. (2003). Selective effects of vagal deafferentation and celiac-superior mesenteric ganglionectomy on the reinforcing and satiating action of intestinal nutrients. Physiol. Behav. *78*, 285–294. https://doi.org/10.1016/s0031-9384(02)00968-x.

53. Magomedova, L., and Cummins, C.L. (2016). Glucocorticoids and metabolic control. Handb. Exp. Pharmacol. *233*, 73–93. https://doi.org/10.1007/164_2015_1.

54. Hunsicker, K.D., Mullen, B.J., and Martin, R.J. (1992). Effect of starvation or restriction on self-selection of macronutrients in rats. Physiol. Behav. *51*, 325–330. https://doi.org/10.1016/0031-9384(92)90148-u.

55. Welch, C.C., Grace, M.K., Billington, C.J., and Levine, A.S. (1994). Preference and diet type affect macronutrient selection after morphine, NPY, norepinephrine, and deprivation. Am. J. Physiol. *266*, R426–R433. https://doi.org/10.1152/ajpregu.1994.266.2.R426.

56. Okamoto, S., Sato, T., Tateyama, M., Kageyama, H., Maejima, Y., Nakata, M., Hirako, S., Matsuo, T., Kyaw, S., Shiuchi, T., et al. (2018). Activation of AMPK-Regulated CRH Neurons in the PVH is Sufficient and Necessary to Induce Dietary Preference for Carbohydrate over Fat. Cell Rep. *22*, 706–721. https://doi.org/10.1016/j.celrep.2017.11.102.

57. Sclafani, A., and Lucas, F. (1996). Abdominal vagotomy does not block carbohydrate-conditioned flavor preferences in rats. Physiol. Behav. *60*, 447–453. https://doi.org/10.1016/s0031-9384(96)80018-7.

58. Buchanan, K.L., Rupprecht, L.E., Sahasrabudhe, A., Kaelberer, M.M., Klein, M., Villalobos, J., Liu, W.W., Yang, A., Gelman, J., and Park, S. (2020). A gut sensor for sugar preference. bioRxiv.

59. Fujita, S., and Donovan, C.M. (2005). Celiac-superior mesenteric ganglionectomy, but not vagotomy, suppresses the sympathoadrenal response to insulin-induced hypoglycemia. Diabetes *54*, 3258–3264. https://doi.org/10.2337/diabetes.54.11.3258.

60. Bohland, M., Matveyenko, A.V., Saberi, M., Khan, A.M., Watts, A.G., and Donovan, C.M. (2014). Activation of hindbrain neurons is mediated by portal-mesenteric vein glucosensors during slow-onset hypoglycemia. Diabetes *63*, 2866–2875. https://doi.org/10.2337/db13-1600.

61. Saper, C.B., and Loewy, A.D. (1980). Efferent connections of the parabrachial nucleus in the rat. Brain Res. *197*, 291–317. https://doi.org/10.1016/0006-8993(80)91117-8.

62. Fulwiler, C.E., and Saper, C.B. (1984). Subnuclear organization of the efferent connections of the parabrachial nucleus in the rat. Brain Res. *319*, 229–259. https://doi.org/10.1016/0165-0173(84)90012-2.

63. Rossi, M.A., and Stuber, G.D. (2018). Overlapping brain circuits for homeostatic and hedonic feeding. Cell Metab. *27*, 42–56. https://doi.org/10.1016/j.cmet.2017.09.021.

64. Craig, A.D. (1995). Distribution of brainstem projections from spinal lamina I neurons in the cat and the monkey. J. Comp. Neurol. *361*, 225–248. https://doi.org/10.1002/cne.903610204.

65. Rinaman, L. (2010). Ascending projections from the caudal visceral nucleus of the solitary tract to brain regions involved in food intake and energy expenditure. Brain Res. *1350*, 18–34. https://doi.org/10.1016/j.brainres.2010.03.059.

66. Palmiter, R.D. (2018). The Parabrachial Nucleus: CGRP Neurons Function as a General Alarm. Trends Neurosci. *41*, 280–293. https://doi.org/10.1016/j.tins.2018.03.007.

67. Herbert, H., Moga, M.M., and Saper, C.B. (1990). Connections of the parabrachial nucleus with the nucleus of the solitary tract and the medullary reticular formation in the rat. J. Comp. Neurol. *293*, 540–580. https://doi.org/10.1002/cne.902930404.

68. Cechetto, D.F., Standaert, D.G., and Saper, C.B. (1985). Spinal and trigeminal dorsal horn projections to the parabrachial nucleus in the rat. J. Comp. Neurol. *240*, 153–160. https://doi.org/10.1002/cne.902400205.

69. Tokita, K., Inoue, T., and Boughter, J.D., Jr. (2009). Afferent connections of the parabrachial nucleus in C57BL/6J mice. Neuroscience *161*, 475–488. https://doi.org/10.1016/j.neuroscience.2009.03.046.

70. Campos, C.A., Bowen, A.J., Schwartz, M.W., and Palmiter, R.D. (2016). Parabrachial CGRP neurons control meal termination. Cell Metab. *23*, 811–820. https://doi.org/10.1016/j.cmet.2016.04.006.

71. Han, W., Tellez, L.A., Perkins, M.H., Perez, I.O., Qu, T., Ferreira, J., Ferreira, T.L., Quinn, D., Liu, Z.-W., Gao, X.-B., et al. (2018). A neural circuit for gut-induced reward. Cell *175*, 665–678. https://doi.org/10.1016/j.cell.2018.08.049.

72. Resendez, S.L., Jennings, J.H., Ung, R.L., Namboodiri, V.M.K., Zhou, Z.C., Otis, J.M., Nomura, H., McHenry, J.A., Kosyk, O., and Stuber, G.D. (2016). Visualization of cortical, subcortical and deep brain neural circuit dynamics during naturalistic mammalian behavior with head-mounted microscopes and chronically implanted lenses. Nat. Protoc. *11*, 566–597. https://doi.org/10.1038/nprot.2016.021.

73. Xu, S., Yang, H., Menon, V., Lemire, A.L., Wang, L., Henry, F.E., Turaga, S.C., and Sternson, S.M. (2020). Behavioral state coding by molecularly defined paraventricular hypothalamic cell type ensembles. Science *370*, eabb2494. https://doi.org/10.1126/science.abb2494.

74. Gunaydin, L.A., and Deisseroth, K. (2014). Dopaminergic Dynamics Contributing to Social Behavior. Cold Spring Harb. Symp. Quant. Biol. *79*, 221–227. https://doi.org/10.1101/sqb.2014.79.024711.

75. Falkner, A.L., Grosenick, L., Davidson, T.J., Deisseroth, K., and Lin, D. (2016). Hypothalamic control of male aggression-seeking behavior. Nat. Neurosci. *19*, 596–604. https://doi.org/10.1038/nn.4264.

76. Gong, R., Xu, S., Hermundstad, A., Yu, Y., and Sternson, S.M. (2020). Hindbrain Double-Negative Feedback Mediates Palatability-Guided Food and Water Consumption. Cell *182*, 1589–1605. https://doi.org/10.1016/j.cell.2020.07.031.

77. Karigo, T., Kennedy, A., Yang, B., Liu, M., Tai, D., Wahle, I.A., and Anderson, D.J. (2021). Distinct hypothalamic control of same- and opposite-sex mounting behaviour in mice. Nature *589*, 258–263. https://doi.org/10.1038/s41586-020-2995-0.

78. Kennedy, A., Kunwar, P.S., Li, L.Y., Stagkourakis, S., Wagenaar, D.A., and Anderson, D.J. (2020). Stimulus-specific hypothalamic encoding of a persistent defensive state. Nature *586*, 730–734. https://doi.org/10.1038/s41586-020-2728-4.

79. Park, Y.G., Sohn, C.H., Chen, R., McCue, M., Yun, D.H., Drummond, G.T., Ku, T., Evans, N.B., Oak, H.C., Trieu, W., et al. (2018). Protection of tissue physicochemical properties using polyfunctional crosslinkers. Nat. Biotechnol. *37*, 73–83. https://doi.org/10.1038/nbt.4281.

80. Ueno, A., Lazaro, R., Wang, P.Y., Higashiyama, R., Machida, K., and Tsukamoto, H. (2012). Mouse intragastric infusion (iG) model. Nat. Protoc. *7*, 771–781. https://doi.org/10.1038/nprot.2012.014.

81. Han, W., Tellez, L.A., Niu, J., Medina, S., Ferreira, T.L., Zhang, X., Su, J., Tong, J., Schwartz, G.J., van den Pol, A., et al. (2016). Striatal Dopamine Links Gastrointestinal Rerouting to Altered Sweet Appetite. Cell Metab. *23*, 103–112. https://doi.org/10.1016/j.cmet.2015.10.009.

82. Schwartz, G.J., Salorio, C.F., Skoglund, C., and Moran, T.H. (1999). Gut vagal afferent lesions increase meal size but do not block gastric preload-induced feeding suppression. Am. J. Physiol. *276*, R1623–R1629. https://doi.org/10.1152/ajpregu.1999.276.6.R1623.

83. Saito, M., and Bray, G.A. (1984). Adrenalectomy and food restriction in the genetically obese (ob/ob) mouse. Am. J. Physiol. *246*, R20–R25. https://doi.org/10.1152/ajpregu.1984.246.1.R20.

STAR★METHODS

KEY RESOURCES TABLE

REAGENT or RESOURCE	SOURCE	IDENTIFIER
Antibodies		
Goat polyclonal anti-Fos	Santa Cruz	Cat# sc-52-g; RRID: AB_2629503
Rabbit anti-CRF	Forver Vale Lab, Salk Institute	Cat# CRF; RRID: AB_2314231
Rabbit anti-alpha-CGRP	Bachem	Cat# T-4032; RRID: AB_518147
Donkey anti-Goat IgG (H+L) Cross-Adsorbed Secondary Antibody, Alexa Fluor 647	Thermo Fisher Scientific	Cat# A-21447; RRID: AB_2535864
Donkey anti-Rabbit IgG (H+L) Highly Cross-Adsorbed Secondary Antibody, Alexa Fluor 594	Thermo Fisher Scientific	Cat# A-21207; RRID: AB_141637
Donkey anti-rabbit IgG (H+L) highly cross-adsorbed secondary antibody, Alexa Fluor 647	Thermo Fisher Scientific	Cat# A-31573; RRID: AB_2536183
Anti-NeuN-antibody	Millipore	Cat# ABN91; RRID: AB_11205760
HA-Tag (C29F4) Rabbit mAb	Cell Signaling Technology	Cat# 3724; RRID: AB_1549585
Goat anti-Chicken IgY (H+L) Cross-Adsorbed Secondary Antibody, Alexa Fluor 488	Thermo Fisher Scientific	Cat# A32931; RRID: AB_2762843
Bacterial and virus strains		
AAV1-CAG-Flex-GCaMP6s-WPRE-SV40	Gift from Dr. Douglas Kim & GENIE Project	Cat# 100835-AAV1; RRID: Addgene_100835
AAV1-CMV-eGFP-Cre-WPRE-SV40	Gift from Dr. James M. Wilson	Cat# 105545-AAV1; RRID: Addgene_105545
AAV5-hSyn-hM4D(Gi)-mCherry	Gift from Dr. Bryan Roth	Cat# 50475-AAV5; RRID: Addgene_50475
AAV1 hSyn FLEx mGFP-2A-Synaptophysin-mRuby	Gift from Dr. Liqun Luo	Cat# 71760-AAV1; RRID: Addgene_71760
AAV2-Ef1a-DIO-ChR2-eYFP	Gift from Dr. Karl Deisseroth	Cat# 35507-AAV1; RRID: Addgene_35507
AAV5-Ef1a-DIO-eYFP	UNC vector core	Cat# AAV5-Ef1a-DIO-eYFP
AAV2-EF1α-DIO-hM4D(Gi)-mCherry	UNC Vector Core	Cat# AAV2-EF1α-DIO-hM4D(Gi)-mCherry
AAV2-hSyn-DIO-mCherry	UNC Vector Core	Cat# AAV2-hSyn-DIO-mCherry
AAV2-Ef1a-DIO-eArch3.0-eYFP	UNC vector core	Cat# AAV2-Ef1a-DIO-eArch3.0-eYFP
AAV1-DIO-RG	Gift from Dr. SeungHee Lee	N/A
AAV1-DIO-TVA-EGFP	Gift from Dr. SeungHee Lee	N/A
pRV-EnvA-ΔG-tdTomato	Gift from Dr. SeungHee Lee	N/A
AAV2/1-hS-FLEX-TVA-HA-N2cG	Kavli Institute for Systems Neuroscience	Cat# AAV2/1-hS-FLEX-TVA-HA-N2cG
EnvA pseudotyped SADB19 Rb mCherry	Kavli Institute for Systems Neuroscience	Cat# EnvA pseudotyped SADB19 Rb mCherry
EnvA pseudotyped N2cG Rb mCherry	Kavli Institute for Systems Neuroscience	Cat# EnvA pseudotyped N2cG Rb mCherry
Chemicals, peptides, and recombinant proteins		
D-glucose	Sigma	Cat# G8270
L-glucose	Carbosynth	Cat# MG05247
D-fructose	Sigma	Cat# F0127
Sucrose	Sigma	Cat# S7903
Sucralose	Sigma	Cat# 69293
Intralipid	Sigma	Cat# I141

(*Continued on next page*)

Continued

REAGENT or RESOURCE	SOURCE	IDENTIFIER
Protein	Proteinex-18	Proteinex-18
Ensure®	Abbott	Ensure® original powder
D-galactose	Sigma	Cat# G0750
D-Mannitol	Sigma	Cat# M4125
Acesulfame K	Supelco	Cat# 04054
Methyl α-D-glucopyranoside	Sigma	Cat# 9376
Cholecystokinin octapeptide (sulfated)	Bachem	Cat#4033010
Peptide Y.Y. (3-36)	Tocris	Cat# 1618
Liraglutide	Tocris	Cat# 6517
Amylin	Tocris	Cat# 3418
Lithium chloride solution	Sigma	Cat# L7026
Ghrelin(rat)	Tocris	Cat# 1465
4OH-tamoxifen	Sigma	Cat# H6278
Clozapine N-oxide (CNO)	Sigma	Cat# C0832
Dexamethasone sodium phosphate	Sigma	Cat# PHR1768
TritonTM-X100	Sigma	Cat# T8787
DAPI	Sigma	Cat# D9542
Nissl stain	Invitrogen	Cat# N21479
Tween® 80	Sigma	Cat# P1754
polyglycerol 3-polyglycidyl ether	Huntsman Corporation	Cat# GE-38
PBS	Nalgene	Cat# AM9625
sodium carbonate	Sigma-Aldrich	Cat# S7795
sodium bicarbonate	Sigma-Aldrich	Cat# S5761
sodium azide	Sigma-Aldrich	Cat# S2002
PBSN	Sigma-Aldrich	Cat# P4417
boric acid	Sigma-Aldrich	Cat# B6768
sodium sulfite	Sigma-Aldrich	Cat# S0505
sodium dodecyl sulfate	Sigma-Aldrich	Cat# 75746
sodium hydroxide	Sigma-Aldrich	Cat# S5881
PES vacuum filter	VWR	Cat# 10040-440
Triton-X	Sigma-Aldrich	Cat# T9284
2,2′-Thiodiethanol	Sigma-Aldrich	Cat# 88561
dimethyl sulfoxide	Alfa-Aesar	Cat# 36480
Normal donkey serum	Abcam	Cat# ab7475; RRID: AB_2885042
Fluorescence Mounting Medium	Agilent	Cat# S3023
Fluoro-Gold	Fluorochrome, LLC	N/A
Silicone Elastomer Sealant	Word Precision Instruments	Kwik-Cast
Ketoprofen	Zoetis	KETOFEN
Enrofloxacin	Baytril®	N/A
Experimental models: Organisms/strains		
Mouse: Crf-IRES-: B6(Cg)-Crh$^{tm1(cre)Zjh/J}$	The Jackson Laboratory	RRID: IMSR_JAX: 012704
Mouse: Crf flox: B Cre 6.129S4(Cg)-Crh$^{tm2.1Maj}$/J	The Jackson Laboratory	RRID: IMSR_JAX: 030110
Mouse: ROSA26iDTR: BL/6-Gt (ROSA)26Sor$^{tm1(HBEGF)Awai}$/J	The Jackson Laboratory	RRID: IMSR_JAX: 007900
Mouse: Ai14: B6.Cg-Gt(ROSA) 26Sor$^{tm14(CAG-tdTomato)Hze}$/J	The Jackson Laboratory	RRID: IMSR_JAX: 007914

(*Continued on next page*)

Continued		
REAGENT or RESOURCE	SOURCE	IDENTIFIER
Mouse: Fos$^{2A\text{-}iCreER}$ (TRAP2): STOCK Fos$^{tm2.1(icre/ERT2)Luo}$/J	The Jackson Laboratory	RRID: IMSR_JAX:030323
Mouse: C57BL/6J	IMSR	C57BL/6J
Software and algorithms		
GraphPad Prism 9.0.2	GraphPad Software Inc., La Jolla, CA	RRID: SCR_002798 https://www.graphpad.com/scientificsoftware/prism/
ImageJ/Fiji	ImageJ Consortium	RRID: SCR_003070 imagej.nih.gov/ij/download/
Zen 2.3	Zeiss	RRID: SCR_013672 https://www.zeiss.com/microscopy/int/products/microscope-software/zen.html
MATLAB 2018b, 2019b	MathWorks	RRID: SCR_001622 https://www.mathworks.com/products/matlab.html
Python 3.0	N/A	RRID: SCR_008394
CaImAn Python toolkit	CaImAn	RRID: SCR_021533Calcium Imaging data Analysis, https://github.com/flatironinstitute/CaImAn
Arduino	Arduino	RRID:SCR_017284 https://www.arduino.cc/en/main/software
Inscopix nVista3.0 HD	Inscopix	RRID: SCR_017407 https://support.inscopix.com/software
ThorImage® LS Software	Thorlabs	https://www.thorlabs.com/newgrouppage9.cfm?objectgroup_id=9072#ad-image-0
StreamPix 7	NorPix	StreamPix, RRID: SCR_015773 https://www.norpix.com/products/streampix/streampix.php
SmartSPIM	LifeCanvas Technologies	SmartSPIM SmartSPIM Light Sheet Microscope
Two photon calcium imaging analysis code	This paper; Github	https://zenodo.org/records/15392507

EXPERIMENTAL MODEL AND STUDY PARTICIPANT DETAILS

Animals

All animal experiments were performed according to protocols approved by KAIST IACUC following the National Institutes of Health guidelines for the Care and Use of Laboratory Animals. We used *Crf-IRES-Cre* mice (B6(Cg)-*Crh*$^{tm1(cre)Zjh/J}$; 012704, Jackson Laboratory), *Crf flox* mice (B6.129S4(Cg)-*Crh*$^{tm2.1Maj}$/J; 030110, Jackson Laboratory), ROSA26*iDTR mice* (BL/6-*Gt(ROSA)26Sor*$^{tm1(HBEGF)Awai}$/J;007900, Jackson Laboratory), Ai14 (B6.Cg-*Gt(ROSA)26Sor*$^{tm14(CAG-tdTomato)Hze}$/J;007914, Jackson Laboratory), and *Fos*$^{2A\text{-}iCreER}$ *(TRAP2)* (STOCK *Fos*$^{tm2.1(icre/ERT2)Luo}$ /J;030323, Jackson Laboratory). All animals (male or female, 8-16 weeks old) were housed individually under a 12-hr dark/light cycle with food and water available *ad libitum* unless specified. For fasted conditions, animals were fasted for 18 hours as noted in the main text; they were maintained *ad libitum* access to water. All mice lines were backcrossed to *C57BL/6J* mice for at least five generations.

For conditional ablation of CRF neurons, *Crf-IRES-Cre* mice were crossed with *ROSA26iDTR* mice. Heterozygous offspring were crossed each other to generate mice with double homozygote for *Crf-IRES-Cre* (homo) mice with iDTR (heterozygote).

METHOD DETAILS

Stereotaxic surgery

Mice were anesthetized with isoflurane (induction, 4%; maintenance, 1-1.5% in 100% O2) and placed under a stereotaxic apparatus (KOPF model 1900). Ophthalmic ointment (Vetropolycin) was applied to the eyes. After hair removal and skin incision, a small hole was drilled according to the coordinates of each target region on the exposed skull. A pulled-glass pipette with a skinny tip filled with AAVs virus and mineral oil was inserted through a small durotomy onto the target regions. The virus (total volume of 100nL∼150nL for the PVN; 300nL∼450nL for the PBN) was injected with a pressure microinjector (Nanoject III, Drummond) at a speed of 30 nL/min. The pipette was held in the target place at least for 10 min after the injection was terminated. The pipette was slowly withdrawn. The coordinates for each target site were calculated according to Paxinos and Franklin mice brain atlas (the 3rd edition).

Stereotaxic coordinates for the viral injection (unless specified)

PVN, AP: -0.75mm, ML: ±0.2mm, DV: -4.72mm (from the skull surface)

LPB, AP: −5.00 mm, ML: ±1.35 mm, DV: −3.50 mm (from the bregma)

The following AAVs and titers were used

AAV1-CAG-Flex-GCaMP6s-WPRE-SV40 (2.0*10∧13 vg/mL), AAV1-CMV-eGFP-Cre-WPRE-SV40 (1.3*10∧13 vg/mL), AAV5-hSyn-hM4D(Gi)-mCherry (7.5*10∧12 vg/mL), AAV1 hSyn FLEx mGFP-2A-Synaptophysin-mRuby (8*10∧12 vg/mL), and AAV1-Ef1a-DIO hChR2(E123A)-EYFP (1.05*10∧13 vg/mL) were purchased from Addgene.

AAV5-Ef1a-DIO-eYFP (3.0x10∧12 vg/mL), AAV1-EF1α-DIO-hM4D(Gi)-mCherry (5*10∧12 vg/mL), AAV2-hsyn-DIO-mCherry (5*10∧12 vg/mL), AAV2-Ef1a-DIO-eArch3.0-eYFP (5*10∧12 vg/mL) were purchased from UNC vector core.

AAV1-DIO-RG; AAV1-DIO-TVA-EGFP (Original D.N.A. plasmid from S.H.L and Packaged in KAIST Bio-Core center) were provided by Dr.Seung-hee Lee's lab and packaged in the KAIST Bio-Core center.

AAV2/1-hS-FLEX-TVA-HA-N2cG (3*10∧11 vg/ml) was purchased from the Viral Vector Core facility of the 674 Kavli Institute for Systems Neuroscience (NTNU).

All viruses were stored in aliquots at -80°C. Viruses with a high original titer were diluted with PBS or noted buffer on the day of use.

For fiber photometry recording of CRF^{PVN} neurons, 120nl of recombinant AAV1-CAG-Flex-GCaMP6s-WPRE-SV40 were unilaterally injected into the PVN of *Crf-IRES-Cre* mice. The mono fiber-optic ferrule (400μm core, 4.9mm of the length, 0.48 NA; Doric lenses) was implanted 300-400μm above the virus injection site (-4.3 mm DV from the skull) and sealed with dental cement (C&B Metabond Quick Adhesive Cement System, Parkell, Japan).

For optogenetic manipulation, the virus was bilaterally injected to the PVN, and a mono fiber-optic cannula (200μm O.D., 4.9mm of the length, 0.48 NA; Doric lenses) was implanted at (A.P: -0.75mm, ML: 0.0mm, DV: 300 μm above the virus injection site) and sealed with dental cement (C&B Metabond).

For conditional knock-out of *CRF* in the PVN, 100-nL of rAAV expressing Cre-GFP were bilaterally injected into the PVN of *CRF flox* ($CRF^{lox/lox}$) or control ($CRF^{lox/+}$) mice.

Animals received intraperitoneal (i.p.) injection of 5 mg/kg ketoprofen, subcutaneous injection of 5mg/kg of Enrofloxacin (Baytril) after the surgery, and were singly housed to recover for 3-4 weeks before testing.

Implantation of GRIN lens

For two-photon calcium imaging of CRF^{PVN} neurons, 120nL of recombinant AAV1-CAG-Flex-GCaMP6s-WPRE-SV40 (1:8 dilution) were unilaterally injected into the PVN of Crf-IRES-Cre mice (AP: -0.72mm, ML: ±0.25mm, DV: -4.73mm), slightly anterior to the lens implantation site to minimize tract within the field of view.

GRIN lens implantation procedure followed the previous report.[72,73] 2-3 weeks after the injection of AAV1-CAG-flex-GCaMP6s, mice were anesthetized with isoflurane, and placed into a stereotaxic apparatus (KOPF 1900). After aseptic skin excision and connective tissue removal, a small hole was drilled around the area of the initial viral injection above the PVN (AP:- 0.75mm, ML: 0.2mm). A fiber tract was created by slowly inserting and withdrawing a blunt steel needle. A ProView GRIN lens (0.6mm of O.D., 7.3mm of the length, Inscopix, PN 100-002171) secured in place with a ProView-implant kit (Inscopix), fitted with a microendoscope (Inscopix), and slowly lowered at AP: -0.75mm, ML: 0.2mm, DV: 150 ∼200μm above the virus injection site.

The ProView GRIN lens position between DV -4.4 and -4.6 mm from the skull surface was adjusted during the surgery by monitoring the fluorescence signals from the miniature microscope (nVista HD v3, Inscopix). The grin lens was secured with C&B metabond once the position was fixed and the microscope apparatus was detached. Around the Proview lens, a custom-made head-fix plate (1cm diameter) was inserted and permanently fixed with dental cement (Ortho-Jet, Lang Dental). Mice were given ketoprofen (5 mg/kg intraperitoneally) and Baytril (5 mg/kg subcutaneously), and left at least one week to recuperate before testing behaviorally.

Fiber photometry recording

The fiber photometry system was constructed as reported previously.[24,74,75] To activate GCaMP6s fluorescence, a 400 Hz sinusoidal 473 nm blue LED light (30μW) (LED. light: M470F1; LED driver: LEDD1B, Thorlabs) was band-pass filtered (passing band: 472±15nm, Semrock, FF02-472/30-25). The emission light from the triggered GCaMP6s fluorescence was sent through a dichroic mirror that reflected 473-nm. A femto-watt silicon photodetector (Newport, 2151) detected band-pass filtered light (passing band: 534 nm, Semrock, FF01-535/50) and recorded it as a digitized signal using a real-time processor (RP2.1, TDT). A 400μm diameter and 0.48 NA patchcord (MFP_400/430/1100-0.48_2.5m_FC-ZF2.5(FP), Doric lenses) connected a fiber implanted to a photodetector system.

Using StreamPix, the real-time signal was time-locked to the same time frame as the video recording system, allowing the acquired signals and the animals' monitored actions to be synchronized. The initiation of intraduodenal infusion was detected in the RP2.1 system by delivering a TTL signal when the syringe pump initiated the infusion.

Analysis of GCaMP signal from fiber photometry

The GCaMP fluorescence signal was normalized as ΔF/F (%) =(F – F0)/F0 × 100 for the peri-event time histograms, where F is the raw GCaMP signal. The average of GCaMP signals during baseline is F0. 10 mins prior to the start of intraduodenal infusion was used as the baseline. The onsets of the infusion were aligned to the time zero.

In bar graphs, the average F/F (percent) was calculated as $(F_{duration}\text{-}F_{baseline})/F_{baseline}$ x100. $F_{baseline}$ is the mean of the baseline GCaMP signal during intraduodenal infusion, and $F_{duration}$ is the mean of the GCaMP signal during the intraduodenal infusion.

The latency to inhibition in Figure S2E was defined as the time window at which GCaMP signal shows statistically different distribution from the baseline GCaMP signal.

The z-score for operant-dry-sipper licking was calculated as ($F_{duration}$ - average of $F_{baseline}$)/standard deviation of $F_{baseline}$. ($F_{duration}$ - average of $F_{baseline}$)/standard deviation of $F_{baseline}$. The baseline was set at 5 secs before the initiation of each licking session. A licking bout is defined as a series of numerous licks within one sec of inter-licking interval. The maximum or minimum z-score within the 10-sec window following the start of each licking bout was noted as *'peak z-score'*

Two-photon *in vivo* calcium imaging

Head-fixed imaging

Mice were habituated to head fixation and fixed static ball with a holding bar for at least three consecutive days and acclimated to the two-photon imaging chamber for 30 mins-1hr/day until mice displayed less struggling with the novel apparatus. On the last habituation day, a plane for field of view (FOV) with adjusting the z-axis and ROI drawings was determined by a two-photon microscope system. A single FOV that captured the most cells was chosen for the stimulus-evoked response session.

Two-photon imaging acquisition

A two-photon microscope (Bergamo II Series Multiphoton Microscopes, Thorlabs) with a fast resonant scanner, a high-sensitivity, phosphide photomultiplier tube (PMT) detector, a tunable laser (Spectra-Physics InSight X3) fixed at 920nm, 20x air objective lens with a working distance of 8.3mm (Olympus LCPLN20XIR, 0.45NA), and multi-axis controller system was used. Imaging acquisition was made in the ThorImage LS Software and ThorSync software with the following sets; 5Hz of imaging session with a frame averaging of 6 from a Fast resonant scanner at 30 Hz; laser power (at the end of the objective lens), 50-130mW, Galvo/Resonance light pathway, gain, 1-2; scan size, 512 x 512; zoom 1. When being compared the images acquired from different sessions, the same FOV was tracked by overlapping the marked representative ROI in the acquisition software and under the same imaging parameters for each mouse. Each recording session per stimulus was continuously recorded for 15-20 mins. The FOV was adjusted along with the drawn ROI, if significantly dislocated after 20-30 mins.

Intraduodenal infusion during calcium imaging

After at least 30 mins of acclimation in the two-photon room, mice were habituated to intraduodenal infusion with water or saline for two consecutive days. Mice were food deprived before each imaging session and given randomized orders of stimuli. In each session, at least two solutions are loaded in the two-channel stainless steel swivels (Instech, 375/D/22), connecting tubing from the syringe pump to the exteriorized tubes on the back of the mice. After each recording session for 15 – 20 mins with a stimulus, a tube was washed with 100-150μL of distilled water during the interval. The other stimulus was given by changing the tube at the back of the mice.

Analysis of GCaMP signal from two-photon imaging

We modified the CaImAn python package's function to analyze the data from the two-photon single cell calcium imaging. The acquired imaging frames were first motion-corrected in a non-rigid manner (NoRMCorre) algorithm. Then the source extraction was performed using a non-negative matrix factorization framework (CNMF) algorithm to extract single cells and their calcium activity traces from the motion-corrected imaging frames. After CNMF, extracted neurons and their calcium traces were manually inspected to avoid possible false positives from motion artifact, overlapping region of interest, optical aberration, and contamination from neuropils.

For longitudinal tracking of extracted neurons in multiple imaging sessions, we used 'register_multisession' function in CaImAn package to extract overlapping neurons from multiple imaging sessions and manually inspected again. Only the neurons that appeared in multiple imaging sessions were registered for further analysis.

For further analysis, calcium traces were z-scored for the baseline fluorescence of each neuron (from 2 mins before the onset of infusion). For the given extracted calcium traces (F(t)), mean (μ) and standard deviation (σ) of F(t) during the baseline period of 2 minutes were calculated, and normalized calcium traces were calculated as z-score, $z(t) = (F(t) - \mu)/\sigma$.

In Figures 4E, 4N, S3E, and S3H, neurons were classified as '*activated*' if the average z(t) during the infusion period exceeded one standard deviation (1σ) compared to the baseline, '*inhibited*' if that average z(t) during the infusion is lower than minus one standard deviation (-1σ) compared to the baseline. '*Other*' includes the neurons that were not 'activated' or 'inhibited' during the infusion period.

In Figures 4F, 4G, 4O, and 4P, for the comparison of individual neuronal activity in response to two stimuli, the neurons that were classified as '*inhibited*' by D-glucose infusion and *'activated'* by L-glucose (Figures 4F and 4G) or lipid (Figures 4O and 4P) infusion were categorized into cluster1 (green). The neurons classified as 'inhibited' by D-glucose infusion and were not classified as 'activated' by L-glucose or lipid infusion were categorized into cluster 2 (blue), while categorized into cluster 3 (red) if vice versa. The neurons that were not classified as 'activated' or 'inhibited' by both stimuli were categorized into cluster 4 (grey).

In Figures 4D and 4M, unsupervised k-means clustering of individual neuronal activity was performed based on the neuronal activity during the infusion. In each neuron, z(t) during the infusion period was normalized by the maximum absolute value of z(t), max(|z(t)|), during the infusion; $z_{norm} = z(t)/ \max(|z(t)|)$.[76] Then the normalized value (z_{norm}) from two different imaging sessions were concatenated into a single column of vector, and 100 times repeated k-means clustering using built-in MATLAB function was performed. The optimal number of clusters was calculated by the *'evalclusters'* function in MATLAB using silhouette clustering evaluation.

In Figures 4H, 4I, 4Q, and 4R, linear binary support vector machine (SVM) decoders were trained to discriminate D-glucose versus L-glucose infusion or D-glucose versus lipid infusion from individual neuronal activity. To decode the infusate type as a function of time (*time-evolving decoder*),[77] z(t) from each imaging session was divided into a 5s bin. Then, the SVM decoder was trained to discriminate the infusate type from neuronal activity in each time bin, and the decoding accuracies were computed using leave-one-out-cross-validation across bouts. The shuffled data were generated by assigning the infusate type randomly to each neuronal. The bar graphs (Figures 4I and 4R) were calculated from average decoding accuracies of the training data, the neuronal activity in each time bin during infusion.

The tuning preference[78] between a pair of stimuli was defined as $(|z_a|+|z_b-|)/(|z_a|+|z_b-|)$, where z_a and z_b represent the average z(t) of each neuron during the infusion of two different infusates such as D-glucose and L-glucose. For this analysis, only neurons that responded (activated or inhibited) to at least one stimulus were used. For instance, in Figures 4J and 4S, only neurons that were classified as 'inhibited' by D-glucose and classified as 'activated' by L-glucose (Figure 4J) or lipid (Figure 4S) were used for the analysis. In Figures S3I–S3N only neurons that were classified as 'activated' at least by one stimulus were used.

Optogenetic activation or inhibition

For the optimal conditions for optogenetic modulation of CRF^{PVN} neuronal activity, we referred to the previous report.[24] Briefly, 100nL of AAV2-EF1a-DIO-ChR2-EYFP (2.0x10∧13 vg/mL) was bilaterally injected into the PVN (Bregma ML: 0.2mm, A.P.: -0.75mm, DV: -4.7 mm from the brain skull) of *Crf-IRES-Cre:Ai14* mice (2-3months). 100nL of AAV2-EF1a-DIO-eArch3.0-EYFP (titers) was bilaterally injected into the PVN. The control mice were injected with AAV5-EF1a-DIO-eYFP (3.0x10∧12 vg/mL). During the surgery, mono fiber-optic cannulas (200μm diameter, 0.48NA, Doric Lenses) were implanted 300-400μm above the target area (ML: 0.0mm, AP:-0.75mm, DV:-4.3mm) and were secured with dental cement (C&B Metabond, S380). Light from a 473nm diode-pumped solid-state (DPSS) laser (CrystaLaser, USA) was delivered through a fiber-optic patch cord (Doric Lenses, Canada) at 10Hz, 10ms of pulse width, 15mW of light intensity at the tip of the optic fiber. Light from a 532nm DPSS laser (CrystaLaser, USA) was continuously delivered with 15mW of light intensity. Light pulses were controlled by a pulse generator (Agilent, USA). For closed-loop optogenetic stimulation, the pulse generator was triggered by TTL signals.

hM4Di-mediated neuronal silencing

To silence CRF^{PVN} neurons, we injected 120nl of AAV1-Ef1α-DIO-hM4Di-mCherry bilaterally into the PVN of *Crf-IRES-Cre* mice. Control animals were those that received bilateral injection with 120nL of AAV2-hSyn-DIO-mCherry. For silencing hM4Di-expressing CRF neurons during the long-term two-choice assay, mice in fed or fasted state were intraperitoneally injected with saline or CNO (5mg/kg, Sigma) dissolved in saline, 30 mins before the assay began. Mice were pair-wisely compared in different sessions with CNO or saline after at least one week of interval. The orders between sessions with saline or CNO were pseudo-randomized among the individuals.

To silence PBNdl neurons while recording CRF^{PVN} neuronal activity, we bilaterally injected 200 nL of AAV5-hSyn-hM4D(Gi)-mCherry into the PBNdl (AP: −5.00mm, ML: ±1.35mm, DV: −3.50mm). CNO (0.3 mg/kg, Sigma) was intraperitoneally injected under brief anesthesia, 30 mins before the baseline recording, followed by ID infusion.

iDTR-mediated ablation of neurons

For ablation of cells expressing CRF *in vivo*, Cre-inducible DTR transgenic mice (iDTR) in which Cre-mediated excision of a STOP cassette allowed cells to become sensitive to diphtheria toxin (DT).[41] iDTR control mice and $Crf\text{-}IRES\text{-}Cre^{(Homo)}$:iDTR mice were administrated two times with the i.p. injection of diphtheria toxin (50 ng/g) with 3 days of intervals, at least one week before the behavior test.

Mono-synaptic retrograde tracing

To mono-synaptically label the inputs to CRF^{PVN} neurons, 250nl of a mixture of AAV-DIO-RG (AAV1, 1.3 * 10∧12 G.C./mL) and AAV-DIO-eGFP-2A-TVA (AAV2, 2.8 * 10∧12 G.C./mL) was unilaterally injected into the PVN of *Crf-IRES-Cre* mice under the stereotaxic apparatus (KOPF1900). 14-days later, pRV-EnvA-ΔG-tdTomato (8.2 * 10∧7) was injected to the marked location of the PVN. 7 days after the rabies virus injection, mice were perfused with saline followed by 4% of PFA for histological analysis. For fasting-induced cFos, mice were food-deprived overnight before perfusion. Brains were sectioned at 50μm with four serial series and further stained or mounted for imaging.

To mono-synaptically label the inputs to PBNdl neurons, 300∼450nL of helper virus (AAV2/1-hS-FLEX-TVA-HA-N2cG, 3*10∧11 vg/mL) was unilaterally injected into the PBNdl of $Fos^{2A\text{-}iCreER}$ mice under the stereotaxic apparatus (KOPF1900). Two weeks later, mice injected with helper virus were fasted for 18 hours and then injected with 4-OHT. One week later, the engineered rabies virus (EnvA pseudotyped SADB19 Rb mCherry; 300∼450nL, 4*10∧8 vg/mL or EnvA pseudotyped N2cG mCherry; 300∼450nL, 1*10∧7 vg/mL, the Viral Vector Core facility of the 674 Kavli Institute for Systems Neuroscience, NTNU) was injected to the marked location of the PBN. Eleven days after the rabies virus injection, mice were perfused with saline followed by 4% of PFA for histological analysis.

Whole spinal cord processing and optical clearing

After the trans-cardiac perfusion, the dissected spinal cords of mice used for the monosynaptic retrograde tracing were post-fixed in 4% PFA in PBS for 48 hours at 4 °C with gentle shaking. Next, the tissues were processed for tissue protection and clearing by using SHIELD.[79] The tissues were incubated in SHIELD-OFF solution (20% (v/v) P3PE (GE-38, Huntsman Corporation, USA) in 1X PBS (AM9625, Nalgene, USA)) for 96 hours at 4 °C with gentle shaking with a change of the solution. The tissues were then subsequently incubated in SHIELD-ON solution (50 mM sodium carbonate (S7795, Sigma-Aldrich, USA), 50 mM sodium bicarbonate (S5761, Sigma-Aldrich, USA), and 0.02% (w/v) sodium azide (S2002, Sigma-Aldrich, USA) in distilled water) at 37 °C for 24 hours with gentle shaking. The tissues were washed with PBSN (0.02% (w/v) sodium azide in 1X PBS (P4417, Sigma-Aldrich, USA)) at room temperature overnight.

Next, the SHIELD-processed tissues were passively de-lipidated in 40 mL of de-lipidation solution (10 mM boric acid (B6768, Sigma-Aldrich, USA), 100 mM sodium sulfite (S0505, Sigma-Aldrich, USA), and 300 mM sodium dodecyl sulfate (75746, Sigma-Aldrich, USA) in distilled water, titrated to pH 9 using 4 M sodium hydroxide (S5881, Sigma-Aldrich, USA), then filtered using 0.2 μm PES vacuum filter (10040-440, VWR, USA)) at 45 °C for 11 to 14 days. After de-lipidation, the SHIELD-processed tissues were incubated in 1% PBSTN (1% (v/v) Triton-X (T9284, Sigma-Aldrich, USA) in PBSN) at 37 °C for 3 days. After 1% PBSTN incubation, the SHIELD-processed tissues were incubated in PBSN at room temperature to eliminate SDS and Triton-X remnants in the samples.

The de-lipidated SHIELD-processed tissues were incubated in optical clearing solution (OCS; 7.49 M 2,2'-thiodiethanol (88561, Sigma-Aldrich, USA), 10.55 M dimethyl sulfoxide (36480, Alfa-Aesar, USA), and 3.23 M iohexol in distilled water) before imaging. The SHIELD-processed tissues were first incubated in 0.5X OCS (OCS : PBSN = 1 : 1) at room temperature overnight. Next, the SHIELD processed tissues were incubated in degassed OCS at room temperature overnight.

Whole spinal cord fluorescence imaging

Optically cleared and mounted tissue samples were imaged using a dynamically axially swept light sheet microscope (SmartSPIM; LifeCanvas Technologies, USA) attached with a 3.6X objective lens (NA = 0.2; 1.8 μm/pixel) and a 2048 × 2048 CMOS camera. 488 nm, 561 nm, and 647 nm illumination channels were used for whole tissue imaging.

Intraduodenal catheter implantation

Intraduodenal catheter implantation was modified from the procedure previously described.[80,81] Surgical areas were shaved with hair-removal cream and cleaned with betadine and ethanol after mice were anesthetized with 1-2% isoflurane inhalation. To externalize the catheter on the back, a midline abdominal skin incision was made, followed by a second incision between the scapulae. Through a midline incision, the stomach was exteriorized and held up to expose the duodenum. The tip of catheter tubing (0.5mm ID * 1mm O.D.) was implemented into the duodenum and sealed by 6-0 non-absorbable Ethicon Prolene suture through a puncture in the duodenum. Saline was injected into the catheter to confirm that no leakage occurred. The catheter was then sutured through an abdominal muscle layer puncture and tunneled subcutaneously to the intracapsular skin, and then the incision on the back was closed. The outer tip of catheter was capped. Post-operatively, mice were treated with a subcutaneous injection of Enrofloxacin (5 mg/kg) and ketoprofen (5 mg/kg), and allowed for at least 7-days before the intraduodenal infusion experiments. To prevent clogging of the catheter, 100μL of saline was daily injected into the catheter before and after the ID infusion.

Infusions with a syringe pump

Each infusate was prepared freshly before the experiment. Catheters implanted onto the duodenum were utilized to administer all liquids with a syringe pump (Harvard Apparatus, 70-4504, pump 11 elite). Each infusion was delivered at a speed of 15μl/min for a total volume of 600μL over 40 mins (for fiber photometry and monosynaptic anterograde tracing experiments) or over 10 mins (for two-photon calcium imaging experiment). Mice were anesthetized with 1-2% isoflurane inhalation during the ID infusion for monosynaptic anterior tracing. Before the fiber photometry and two-photon calcium imaging experiments, animals fitted with a catheter were given at least two days of habituation with distilled water infused into the duodenum.

Drug and hormone treatments

CCK (10 μg/kg), PYY (0.1 mg/kg), liraglutide (0.4 mg/kg), and Ghrelin (60 μg/mouse) were administered by intraperitoneal (i.p.) injection (at a volume of 10 μL/g body weight).[6] Animals were habituated in the recording chamber for 30 min prior to injection. I.P. injection was administered under a brief anesthesia with isoflurane. Fiber photometry recording continued for 30 mins or longer as indicated. For the onset of PSTH, the moment at which the investigator opened the behavioral chamber defined as the treatment onset.

For the blockades of glucose transport, 0.4% of phloridzin (SGLT1/2 blocker) and 0.23 % of phloretin (GLUT2 blocker) were dissolved in 30% of glucose solution mixed with 3.25% NaOH.

Video recording and behavioral analysis

All behavioral experiments were performed in a custom-made behavior chamber with an air fan and under dimmed light or infrared illumination from the start of the dark cycle. Mice were habituated in the chamber for 20 mins before each experiment. Their behaviors were videotaped using two synchronized infrared cameras (Basler, ace120gc) placed from the top/side of the chamber and

commercial acquisition software (StreamPix 7, Norpix) at a frame rate of 25 frames/s. Manual behavior annotation was executed on a frame-by-frame basis with Caltech behavior annotator code written in MATLAB3. The behavior annotation was time-locked with the recorded GCaMP6 signal and plotted as a bar plot under its trace using MATLAB.

Two-bottle preference assay

Single-housed mice were pre-acclimated to two water bottles with drinking spouts in their home cage for three days. Mice were habituated in a behavior apparatus (20 x 20 x 20cm) with two bottles connected to a sound-attenuated custom-designed lickometer (Arduino UNO). An adaptation session was considered successful if there was no lateral bias toward either sipper (preference index less than 25%) and at least 200 licks were obtained within 30 minutes. Then the mice are placed in their home cage for one day and fed *ad libitum*. Mice were housed in new bedding cages and fasted for 18–20 h, with free access to water. For testing, mice were acclimated in the behavioral chamber box for 20 min and then placed in an apparatus containing two bottles containing either 100 mM sucrose or 0.5 mM sucralose. All behavioral experiments were videotaped and recorded 1∼2 hours after the start of the dark cycle, and were only tested on naïve mice that consumed sugar for the first time.

For optogenetic manipulation during the two-choice assay, an automated lickometer was custom-designed to deliver TTL signals to the pulse-generator to turn on the optic laser (532nm) or to pair with the detected lickings for photoinhibition. In Figures 3K–3N, 5 sec of 10ms width, 10Hz laser pulses were synchronized with the onset of lick. Another lick during 5 secs of photoinhibition did not trigger additional photoinhibition.

Preference index (%); percentage of the total licks for sucrose or sucralose = $(Lick_{Sucrose} - Lick_{Sucralose})/(Lick_{Sucrose} + Lick_{Sucralose})$ x 100. The raw data from the lickometer was used to investigate licking dynamics using custom-designed MATLAB code.

Operant conditioning of self-infused nutrients

To receive the intraduodenal infusion, mice were trained to lick a dry metallic spout. The training procedure modified from the previously reported operant dry-sipper licking protocols.[14,39] Mice implanted with a catheter in the duodenum were given a spout baited with chow under food restriction during training. To train mice to lick the dry spout, a small piece of chow pellet was placed below the opening of the spout (mice can smell but cannot ingest the pellet) and Ensure (0.6 kcal/ml) was infused for 3 seconds at 100μL /min to the duodenum whenever the mice licked the dry spout. Another lick during the 3-sec infusion was counted but did not trigger another infusion. The training session lasted an hour for three days in a row under food restriction (maintaining 80% of body weight). Over 300 licks every session was considered successful. The trained mice were overnight fasted for a test session. An empty dry spout was presented during the test session, where a detected lick triggered the infusion of D glucose (30%), lipid (13.3%, isocaloric to % D-glucose), or L-glucose (30%) at the same rate and duration as the training session. TTL signals were sent from all detected licks to the TDT recording system, which were aligned with GCaMP6 signals for the analysis. TTL signals were also sent to pulse-generators and an infusion pump once the lick-paired optogenetic activation system detected a lick from a dry spout. The 5 sec of 10ms width, 10Hz laser pulses were synchronized with the start of 3 sec intraduodenal infusion. Another lick during the 5 secs of stimulation did not trigger an additional stimulation.

Subdiaphragmatic vagotomy

As previously reported,[82] mice were anesthetized with 2% isoflurane inhalation and placed on a heating pad. Then surgical sites were shaved with hair-removal cream and cleaned with betadine and ethanol. A midline abdominal incision was made along 1.5cm below the xiphoid process. The stomach was exposed to the abdominal cavity and kept moisturized with a piece of tissue soaked with sterile saline. The liver was delicately retracted to the right side by gently removing all connective tissues between the liver and the stomach. Then, the subdiaphragmatic portion of the esophagus was exposed, and the anterior and posterior trunk of the vagus nerve was identified above the hepatic branch. Both identified nerves were dissected from the esophagus, hooked up, and burned with a high-temperature cautery fine tip (Bovie) to prevent potential regeneration of the vagal nerve. We used the mice that received the intraduodenal tubing implementation as sham mice because of the similarity of the surgical procedure. At the end of the surgery, mice were given Baytril (5 mg/kg) and ketoprofen (5 mg/kg) and allowed for at least one week of recovery before further experiment. During five days after the vagotomy, mice were provided with liquid food to assist their gastric motility or other possible gastrointestinal issues. Vagotomized mice that had received intraperitoneal injections of Fluorogold (20 mg/kg in saline; Fluorochrome), which retrogradely labeled the vagal neurons in the DMV, were sacrificed after 4 to 6 days of injection and confirmed the absence of Fluorogold in the DMV.

Celiac-superior mesenteric ganglionectomy

Mice were anesthetized with 1∼2% of isoflurane inhalation on a heating pad, and a ventral abdominal midline incision was made, as previously reported.[52] The abdominal cavity was exposed by retracting the intestines to the right side. The left adrenal cortex, kidney, descending aorta, celiac arteries (CA), and superior mesenteric arteries (SMA) were located as a hallmark of the surgical area. The anterior and posterior celiac ganglion and superior mesenteric ganglion were identified and denervated by gently removing all connections between the CA and SMA. At the end of each surgery, the image of post-surgery was photo-captured. Retracted intestine tissues were placed back, and the abdominal incision was closed. After a week of recovery with the post-surgical treatment of Baytril (5 mg/kg), the same mice received the duodenal catheter implantation.

Adrenalectomy

Mice were anesthetized with 2% isoflurane inhalation and placed on a heating pad. Then surgical sites were shaved with hair-removal cream and cleaned with betadine and ethanol. Bilateral incisions were made below the scapula and abdomen at the side, and the second incision was made on the muscle wall. After locating the kidneys, the adrenal gland with the attached fat pad was individually pulled out. The muscle wall and skin were sutured tightly. The same procedure was conducted at the other side for the bilateral adrenalectomy. For the post-surgery supplementation of sodium, mice were provided with 0.9% NaCl in drinking water post-operationally.[83]

Post-surgical care

Post-surgery mice were placed over a heating pad and monitored for their recovery from anesthesia. All mice were given post-surgery analgesia by subcutaneous injection of Enrofloxacin (Baytril, 5 mg/kg) on post-surgery day 2 and day 3. After GRIN lens implantation surgery, dexamethasone (4 mg/L) was provided in drinking water for one week.

FluoroGold injection

FluoroGold (Fluorochrome) was injected at 20 mg/kg intraperitoneally to retrogradely label vagal efferent neurons in the D.M.V. 4-7 days following the injection, animals were euthanized, and labeled tissue was harvested for the histology.

Immunohistochemistry

Animals were anesthetized with isoflurane and cordially perfused with 30ml of 4% PFA following 30ml of 0.9% saline. Brains and spinal cords were post-fixated for 4 hrs in 4% PFA at 4°C and then transferred to 20% and 30% sucrose in PBS serially. Brains were coronally sectioned at 50μm using a Leica cryostat. The sectioned brains were washed with PBS for 10 mins and blocked with 2% normal donkey serum in 0.2% PBST for 1 hr at R.T. Primary antibodies; rabbit anti-CRF (1:250, Vale lab, PBL rC68) or goat anti-cFos (1:200, Santa Cruz, sc 52-g) antibody in the blocking solution (2% NDS in 0.2% PBST-Triton X-100) were incubated at 4°C for 72-hrs or 24-hrs, respectively. The sections were washed with PBS (3 x 15 mins), followed by incubation of second antibody - donkey anti-rabbit Alexa 647 (1:500, Life Technologies, A21207) or donkey anti-goat Alexa 488 (1:500, Life Technologies, A11055) for 1 hr at RT and then were washed with PBS (2 x 15 mins), stained with DAPI (1:10000) for 6 mins, and mounted with DAKO mounting medium. The jugular-nodose ganglia (NG) were dissected from perfused mice and fixed with 4% PFA for 4hr. The whole nodose ganglia were washed with PBS (3X15mins) and blocked with 3% normal donkey serum in 0.3% PBST for 1 hr at RT. Primary antibodies; Anti-NeuN-antibody (1:500, Sigma Aldrich, ABN91) in the blocking solution (3% NDS in 0.3% PBST-Triton X-100) were incubated at room temperature for 24 hrs. The tissue were washed with PBS (3 x 15 mins), followed by the incubation with second antibody - Goat anti-Chicken Alexa 488 (1:500, Invitrogen, A32931) for 1 hr at RT and then were washed with PBS (2 x 15 mins), stained with DAPI (1:20000) for 10 mins, and mounted with DAKO mounting medium. Spinal cords were coronally sectioned at 80μm using a Leica cryostat. The sectioned spinal cords were washed with PBS (3X15mins), stained with Nissl (1:500) for 3 hrs at RT, and mounted with DAKO mounting medium. Confocal images were captured with a Zeiss LSM 780 microscope and analyzed using Image J.

QUANTIFICATION AND STATISTICAL ANALYSIS

All statistical analyses were performed with GraphPad Prism 9.0.2. To compare two groups that present the normal distribution, unpaired two-tailed t-tests were conducted. For multiple comparisons between the groups representing the normal distribution, one-way ANOVAs followed by Tukey's post hoc test were performed (see Table S1). Data are presented as Mean ± SEM. When we conducted the one-way ANOVAs followed by Tukey's post hoc test, the absence of an asterisk refers non-significant ($P > 0.05$).